HHS Public Access

Author manuscript

Nat Immunol. Author manuscript; available in PMC 2024 January 01.

Published in final edited form as:

Nat Immunol. 2023 June ; 24(6): 1036–1048. doi:10.1038/s41590-023-01501-5.

Dynamic chromatin accessibility licenses STAT5- and STAT6-dependent innate-like function of Th9 cells to promote allergic inflammation

Aran Son[1], **Francoise Meylan**[2], **Julio Gomez-Rodriguez**[3,4], **Zenia Kaul**[3], **McKella Sylvester**[1], **Guido H. Falduto**[5], **Estefania Vazquez**[1], **Tamara Haque**[1], **Moses M. Kitakule**[1,6], **Chujun Wang**[5], **Kalpana Manthiram**[3], **Chen-Feng Qi**[7], **Jun Cheng**[8], **Rama K. Gurram**[3], **Jinfang Zhu**[3], **Pamela Schwartzberg**[3], **Joshua D. Milner**[6,*], **Pamela A. Frischmeyer-Guerrerio**[1,*], **Daniella M. Schwartz**[1,5,*]

[1]Laboratory of Allergic Diseases, National Institute of Allergy and Infectious Diseases, National Institutes of Health

[2]Office of Science and Technology, National Institute of Arthritis, Musculoskeletal, and Skin Diseases, National Institutes of Health

[3]Laboratory of Immune System Biology, National Institute of Allergy and Infectious Diseases, National Institutes of Health

[4]TCR Therapeutics, Inc. Cambridge, MA

[5]Division of Rheumatology and Clinical Immunology, University of Pittsburgh

[6]Division of Pediatric Allergy Immunology and Rheumatology, Department of Pediatrics, Columbia University Medical Center

[7]Pathology Core, Laboratory of Immunogenetics, National Institute of Allergy and Infectious Diseases, National Institutes of Health

[8]Embryonic Stem Cell and Transgenic Core, National Human Genome Research Institute, National Institutes of Health

Abstract

Allergic diseases are a major global health issue. Interleukin-9 (IL-9) producing T helper cells (Th9) promote allergic inflammation, yet Th9 effector functions are incompletely understood because their lineage instability makes them challenging to study. Here, we found that resting

Corresponding author: Daniella M. Schwartz, MD, University of Pittsburgh, Division of Rheumatology and Clinical Immunology, BST S719, 200 Lothrop St., Pittsburgh, PA 15213, Daniella.Schwartz@pitt.edu.

*These authors contributed equally

Author Contribution Statement

FM and JG-R contributed equally to this manuscript. AS, FM, J G-R, ZK, MK, MS, GF, CW, TH, EV, JC, DMS, and CFQ performed experiments and analyzed data. KM and JDM provided patient samples. RG and JZ provided proprietary reagents. AS and DMS authored the manuscript. JDM, PS, PFG, and DMS provided supervision.

Competing Interests statement

J G-R is currently employed by TCR Therapeutics. All the other authors have no interests to declare.

Data and software availability

Raw and analyzed data are available on GEO, accession number GSE222910.

Th9 cells produced IL-9 independent of TCR restimulation, due to STAT5- and STAT6-dependent bystander activation. This mechanism was seen in circulating cells from allergic patients and was restricted to recently activated cells. STAT5-dependent *Il9/IL9* regulatory elements underwent remodeling over time, inactivating the locus. A broader "allergic Th9" transcriptomic and epigenomic program was also unstable. *In vivo,* Th9 cells induced airway inflammation via TCR-independent, STAT-dependent mechanisms. In allergic patients, Th9 expansion was associated with responsiveness to JAK inhibitors. These findings suggest that Th9 instability is a negative checkpoint on bystander activation that breaks down in allergy, and that JAK inhibitors should be considered for allergic patients with Th9 expansion.

Introduction

Allergic diseases affect up to 40% of the global population and cause substantial morbidity and mortality; understanding the drivers of allergic pathology is critical to devising effective therapies[1]. T helper 9 (Th9) cells are implicated as major mediators of allergic disease through production of interleukin-9 (IL-9)[2]. *IL9* polymorphisms are associated with allergic disease risk; Th9 expansion is seen in asthma, atopic dermatitis, and food allergy; and Th9 cells exacerbate murine models of allergic disease[3-8]. IL-9 promotes allergic inflammation by inducing mast cell maturation, enhancing immunoglobulin E production, recruiting eosinophils and neutrophils, promoting mucous cell metaplasia, and increasing epithelial permeability[5,9-11]. Additionally, Th9 cells have emerged as major drivers of autoimmunity and antitumor immunity[2,10-14].

Despite the importance of Th9 cells to this broad cross-section of inflammatory diseases, they are incompletely characterized. This is partly because Th9 cells are extremely heterogeneous, but also because they display unique lineage plasticity and effector kinetics: their capacity for IL-9 production decreases over time[9,10,15-18]. The factors constraining Th9 stability are poorly understood, with most studies focusing on mechanisms of Th9 differentiation[17,19-22]. Because the "Th9" phenotype disappears shortly after *in vitro* T cell receptor (TCR) stimulation is withdrawn, it has been suggested that Th9 lineage stability requires sustained TCR signaling[16,23]. However, TCR-dependent transcription factors (TFs) have not been found to enhance Th9 stability[20-22]. Other Th9-promoting TFs include STAT5 and STAT6, which bind to critical *cis*-regulatory elements (REs) in the *IL9* locus and increase accessibility during differentiation[16,24-27]. STAT5 signaling also enhances TCR-stimulation and activation of effector Th9 cells[28]. These observations suggest that STAT-dependent cytokines might contribute to the unique kinetics of Th9 lineage commitment and function.

Here, we found that paracrine IL-2 and IL-4 induced bystander activation of resting Th9 cells through STAT5 and STAT6, independent of TCR-restimulation. Critical STAT5-/STAT6-binding *IL9 cis*-regulatory elements (REs) became poised for transcriptional induction during Th9 differentiation. RE accessibility slowly decreased after withdrawal of TCR stimulation, repressing STAT5-target expression and causing instability of the Th9 phenotype. *In vivo*, pulmonary Th9 underwent TCR-independent, STAT-dependent activation to promote allergic lung inflammation. In patients with allergic disease, Th9

expansion was associated with STAT5 induction, STAT6 induction, and responsiveness to JAK inhibitors (jacanids). Our findings link the epigenetic mechanisms underlying Th9 instability to STAT-dependent bystander activation. These activation mechanisms may have a role in antihelminth responses, where antigen-specific responses are suppressed, while simultaneously providing a negative checkpoint that breaks down in patients with allergic diseases[29]. Therefore, STAT-dependent Th9 bystander activation may underlie a novel allergic endotype that predicts jakinib-responsiveness, and JAK inhibitors should be considered for allergic patients with a Th9 signature.

Results

Bystander Th9 activation drives persistent IL-9 secretion

To determine how IL-9 kinetics might be affected by TCR activation, we purified naïve human $CD4^+$ T cells and cultured them with TCR-stimulation (αCD3, αCD28), IL-2, and cytokines/neutralizing antibodies to promote Th1, Th2, or Th9 differentiation. After d5 of culture, we withdrew TCR-stimulation, resting the cells in IL-2 and subset-promoting cytokines/antibodies (Fig 1a). Resting Th1 and Th2 cells produced effector cytokines only upon short (6-hour) restimulation with TCR mimetics (Fig 1b-c**, S1a-e**). By contrast, resting Th9 cells produced IL-9 without restimulation, even after resting for 6 days (Fig 1b-c**, S1f**). In murine Th9 cells, IL-9 production was detectable without restimulation after resting for 2 days (Fig 1d-f**, S1g-k**).

These findings led us to hypothesize that paracrine cytokines might promote bystander activation of Th9 cells. To test this, we stimulated *in vitro*-differentiated human Th1, Th2, and Th9 cells with αCD3, collected supernatants, and used supernatants to stimulate d8-resting Th9 cells. All three supernatants induced IL-9, suggesting that resting Th9 cells undergo bystander activation downstream of paracrine cytokines (Fig 1g-h). Bystander activation of Th1 and Th2 cells is induced by IL-1-family cytokines through NF-κB and p38MAPK and enhanced by STAT-dependent cytokines[30]. We hypothesized that similar mechanisms might induce IL-9: IL-1β and IL-2 blockade reduced supernatant-induced IL-9 induction (**Fig S1l**). Because IL-1β enhances Th9 responsiveness to IL-2[31], we also treated resting Th9 cells with IL-1 family cytokines alone. IL-1β, IL-18, IL-33, IL-36α, and IL-36γ failed to induce IL-9, suggesting that these cytokines do not induce bystander Th9 activation (**Fig S2a**). Moreover, NF-κB (BAY11) and p38MAPK (CAY10571) inhibition had only a moderate effect on supernatant-induced IL-9 production (Fig 1i-j). NFAT signaling blockade (FK506) also had a modest effect, but JAK-STAT inhibition (tofacitinib) profoundly repressed supernatant-induced IL-9 production (Fig 1i-j). Together, these results indicated that STAT-dependent paracrine cytokines induce bystander activation of resting Th9 cells.

STAT5 and STAT6 induce Th9 bystander activation

We next sought to identify the specific cytokines and TFs underlying Th9 bystander activation. STAT5 and STAT6 are critical for Th9 differentiation and function[16,25]; d8 $IL\text{-}9^+$ cells exhibited high STAT5 and STAT6 phosphorylation (Fig 2a-b), and STAT5 and STAT6 inhibitors reduced IL-9 production in d8 Th9 cells (**Fig S2b-c**). Th9-promoting STAT5- and

STAT6-activating cytokines include TSLP, IL-7, IL-2, IL-4, and IL-9[7,17,21,25,27]. Because TSLP and IL-7 derive from non-hematopoietic cells[7,32], we measured IL-2, IL-4, and IL-9 concentrations in Th1, Th2, and Th9 supernatants. We detected all three cytokines (**Fig S2d-f**), leading us to hypothesize that they might promote Th9 bystander activation. IL-2 and IL-4 induced IL-9, whereas IL-9 and other STAT-dependent cytokines had no effect (Fig 2c-d**, S2g-k**). STAT5 and STAT6 phosphorylation were induced in cytokine-treated IL-9$^+$ cells (**Fig Sl-m)**. JAK-STAT, STAT5, and STAT6 inhibition prevented cytokine-induced IL-9 production (Fig 2e-f**, S2n**).

These findings led us to question whether similar mechanisms could activate *in vivo*-generated human memory Th9 cells [3,4,6]. Treatment with IL-2 and IL-4 induced IL-9 in circulating CD45RO$^+$CD4$^+$ T cells from atopic dermatitis patients but not healthy volunteers (Fig 2g-h). Th9 cells can also be identified in lymphoid tissues, where they promote germinal center development[33]. Treatment with IL-2 and IL-4 induced IL-9 in human tonsil-derived CD4$^+$CD45RO$^+$ T cells (Fig 2g-h). Together, these results demonstrate that IL-2 and IL-4 induce bystander activation of resting human Th9 cells through STAT5 and STAT6.

Th9 bystander activation occurs via transcriptional induction

Acute cytokine induction can occur via transcriptional induction or post-transcriptional regulation[34]. Because STAT5 and STAT6 are Th9-promoting TFs[16], we hypothesized that STAT-dependent Th9 bystander activation occurred through transcriptional induction. Accordingly, treatment with IL-2 and IL-4 induced *IL9* total mRNA and nascent (newly synthesized) mRNA (Fig 3a-b). These results suggested that STAT5 and STAT6 rapidly and directly target the *IL9* locus to promote bystander activation.

Bystander activation is restricted to recently activated Th9

Because STAT-dependent regulation of cytokine loci is also important for T helper lineage commitment, we next asked whether the mechanisms underlying Th9 lineage instability might prevent nonspecific Th9 bystander activation in healthy subjects. To address this, we followed human and murine *in vitro* Th9 differentiation through an extended time course (Fig 3c-f**, S3a-d**). Although murine Th9 cells lost IL-9-effector capacity by d7, 10-20% of human Th9 cells retained the ability to produce IL-9 (**Fig S3a-d)**. IL-9 production was highest in cells restimulated with a combination of IL-2 + IL-4 (STAT-activators) and PMA + ionomycin (TCR-mimetics), suggesting that the mechanisms are additive (**Fig S3b,d**). We therefore hypothesized TCR and STAT agonists might additively induce IL-9 in circulating human Th9 cells. Stimulation of PBMCs from atopic dermatitis patients with STAT-dependent cytokines enhanced the effect of TCR-mimetics, suggesting bystander activation is required for optimal human Th9 function (**Fig S3e-f**).

Although some human Th9 cells exhibited lineage stability, cytokine-dependent IL-9 induction was limited to recently activated human and murine Th9 cells and could not be seen after prolonged resting (human d15, mouse d6, Fig 3c-f**, S3a,c**). This could be due to Th9 lineage instability or death of IL-9-producing clones. We therefore sorted d3-*in vitro* differentiated IL-9$^+$CD4$^+$ cells from IL-9 reporter (INFER) mice and rested them over time[9].

These remained viable but lost capacity to make IL-9, confirming that transient effector kinetics are related to lineage instability (Fig 3g**, S3g-h**). Taken together, these findings indicate that bystander IL-9 induction is limited to recently activated Th9 cells and that Th9 lineage instability may prevent nonspecific STAT-dependent bystander activation under homeostatic conditions.

The Th9 transcriptional program is unstable over time

To better understand the link between Th9 lineage instability and STAT-dependent bystander activation, we first set out to better delineate the transcriptional program characterizing Th9 cells. Prior transcriptomic analyses of IL-9-producing T cells have yielded conflicting results about the identity of these cells, with some studies indicating they are a distinct T helper subset and other studies suggesting they may be a group of early activated Th2 cells[15-17,23]. To resolve some of these questions, we integrated data from four transcriptomic datasets profiling *in vivo* Th9 cells[15,16,23]. Two datasets profiled lung-resident Th9 cells from IL-9-reporter mice exposed to intranasal papain, one profiled circulating Th9 clones from healthy volunteers, and one profiled house dust mite (HDM)-reactive Th9 cells from allergic asthma patients[15,16,20,23]. We also used one dataset comparing *in vitro*-differentiated Th9 with 4 other T helper subsets[16]. Overlap of DEGs between the various datasets was low, reflecting the heterogeneity of IL-9$^+$ T cells in various contexts and models. Nonetheless, we defined a cassette of 175 “allergic Th9” genes that were differentially expressed in IL-9$^+$ T cells in ≥2 datasets (**Fig S3i,** Extended Data Table 1). In addition to *Il9*, this cassette included several canonical Th2 genes (*Il4, Il5, Il13, Ccr4*) and “IL9$^+$ Th2” genes linked to early/activated IL-9$^+$ Th2 cells (*Ccl17, Ccr8, Pparg*). A group of “IL9$^+$ non-Th2” genes was also seen, which are not typically expressed in the Th2 lineage (*Spi1, Gzmb, Csf2*). We further validated the “allergic Th9” cassette by testing for net enrichment (Gene Set Enrichment Analysis, GSEA) in multiple public datasets, including antitumor Th9 cells, *IL9*-expressing atopic dermatitis skin, and HDM-stimulated *IL9*-expressing T cells from allergic subjects (Fig 3h). Pathway analysis revealed enrichment for activation, chemotaxis, and cytokine signaling – particularly by IL-1, IL-17, and antiviral cytokines (**Fig S3j**).

We next probed Th9 transcriptomes over an extended time course of differentiation and resting, during which *IL9/Il9* was first induced and then repressed (Fig 3c-f, i-j). The “allergic Th9” cassette was enriched in d3 (murine) and d5 (human) Th9 cells relative to naïve cells (Fig 3h). 589 genes were transiently induced in both murine Th9 (FC >2, FDR<0.05, d3-d4 vs. d0-d8), and human Th9 (FC>2, FDR<0.05, d5-d8 vs. d0-d15). 26 “allergic Th9” genes were transiently induced, including *Il9/IL9, Il13/IL13*, and *Csf2/CSF2,* but not *Pparg/PPARG*, *Spi1/SPI1*, *Gzmb/GZMB*, or *Ccr8/CCR8* (Fig 3i,j). Net expression of the “allergic Th9” cassette correlated with *IL9/Il9* expression, further suggesting that this program is unstable (Fig 3k,l). Net expression of STAT5-induced genes also correlated with *IL9/Il9* expression; weaker enrichment was seen for STAT6-induced genes (**Fig S3k**). STAT1 and STAT3 are reported to antagonize Th9 differentiation by competing with each other and with STAT5[35-37]; STAT1-induced genes inversely correlated with *IL9/Il9* expression in murine and human cells, suggesting a potential role in Th9 instability (**Fig S3k**).

Chromatin remodeling promotes Th9 lineage instability

Global chromatin architecture provides an unbiased view of T helper identity that can be more stable than gene expression[38]. To determine how Th9 identity changes over time, we measured accessibility (ATAC-seq) and histone marks for *cis*-regulatory elements (REs): poised enhancers (H3K4Me1), active promoters (H3K4Me3) and active enhancers (H3K27Ac). We probed epigenomes over a time course of differentiation and resting in human and murine *in vitro* generated Th9 cells (Fig 3c-f). We identified a set of dynamic peaks that were gained on d3-4 and lost by d8 in murine Th9, or gained on d5-8 and lost by d15 in human Th9, and therefore specific to cells that could undergo bystander activation. "Allergic Th9" gene loci were enriched for dynamic ATAC-seq peaks, indicating that the Th9 lineage is unstable at an epigenetic level (Fig 4a,b). Enrichment for dynamic histone marks was seen in murine Th9 cells but not in human cells, suggesting that the murine Th9 epigenetic program is less stable than the human Th9 program (Fig 4a,b).

We next sought to identify TFs that might preferentially induce gene expression in recently activated Th9 cells. Binding sites for these TFs should open and gain activating histone marks upon Th9 differentiation, then close and lose histone marks after prolonged resting[39]. We therefore searched for TF motifs with significantly enriched abundance (HOMER) in dynamic peaks. We identified 14 motifs that were enriched in human and murine dynamic peaks; 3 genes encoding for the associated TFs were also induced during Th9 differentiation – *Stat5a/STAT5A*, *Irf4/IRF4*, and *Batf/BATF* (Fig 4c). The STAT5 motif was enriched in 5 dynamic peak groups, representing the most conserved enriched motif, and *Stat5a* expression was dynamically induced in Th9 cells (Fig 4c). Thus, analysis of Th9 epigenomes suggested that chromatin remodeling reduces accessibility and activation of STAT5-binding *cis*-REs over time, even in the presence of IL-2.

Chromatin remodeling represses *Il9/IL9* over time

Having found globally reduced accessibility and activation of STAT5-binding sites over time, we next investigated the *Il9/IL9* locus[16,40-42]. The murine *Il9* locus comprises five STAT5-binding *cis*-REs: a downstream enhancer (DS, also called CNS2, SEa), promoter (*Il9*p), and three upstream enhancers (E1, also cells CNS0, SEb; E2, also called CNS-25, SEc; and E3, also called CNS-25, SEc)[16,40-42] (Fig 4d). *Il9*p, E1, and E2-E3 – previously defined as Th9-specific enhancers – gained accessibility and histone marks in murine d3-Th9 cells relative to naïve-T cells (Fig 4d). *Il9*p accessibility and H3K4me3 were reduced on d4 and absent by d8, whereas E1 and E2 were accessible and bore active enhancer marks on d4 but not d8; poised enhancer marks were also repressed on d8 (Fig 4d). Together, these changes caused the extended *Il9* locus to revert to the naïve state in d8-cells that were refractory to bystander activation. By contrast, other "allergic Th9" loci, including the Th2 (*Il4-Il13-Il5*) and *Gzmb* loci exhibited sustained differences between d8 and d0 (naïve) (**Fig S4a-b**).

By contrast, the human *IL9* locus contained six potential *cis*-REs: a downstream RE (DS), the promoter (*IL9p*), and four upstream cis-REs 5kb upstream of the promoter (Fig 4e). One of these REs was previously described as CNS-18, an enhancer homologous to murine E3[41,42]. One RE (E1) previously described as CNS-4.5 was homologous to murine E1[41,42],

and one RE (E2) located 14kb from the transcription start site was homologous to murine E2. One previously undescribed RE (E4) displayed Th9-specific accessibility relative to naïve cells. DS, *IL9*p, and E1-E4 also displayed Th9-specific accessibility compared to human naïve and *in vitro* differentiated Th1 cells (**Fig S4c**). In *ex vivo* human memory $CD4^+$ cells (ENCODE), DS was accessible in multiple T helper subsets, whereas E3-E4 were specifically accessible in Th2 and Th17 cells, which can acquire IL-9-producing capacity[23,25](**Fig S4d**), indicating that in vivo findings support the functional relevance of these human *IL9*-REs (Fig 4e).

We next compared *IL9* locus architecture in naïve (d0), recently activated (d5-8) cells that can undergo bystander activation, and remotely activated (d15) human Th9 cells. As in murine Th9 cells, certain *cis*-REs within the extended *IL9* locus lost accessibility by d15 (Fig 4e). By comparison, accessibility of the *GZMB* and Th2 (*IL4-IL13-IL5*) loci were sustained through late timepoints in human and murine cells (**Fig S4e-f**). Compared with the murine *Il9* locus, dynamic regulation of the human *IL9* locus was more stable and correlated more strongly with regulation of the Th2 locus (**Fig S4g**).

Together, these findings reveal that the extended *Il9*/*IL9* locus undergoes epigenetic remodeling over time. During Th9 differentiation, the locus opens, allowing TCR-independent STAT5/STAT6-dependent bystander activation. After TCR stimulation is withdrawn, the *Il9/IL9* locus loses accessibility over time, preventing TF binding and resulting in Th9 lineage instability. This mechanism is most pronounced in murine Th9 cells, consistent with the reduced stability of murine Th9 cells compared with human cells.

Pulmonary Th9 cells have an activated transcriptomic signature

Like *in vitro*-generated and circulating Th9 cells, lung-resident Th9 cells have transient effector functions[18,23]. We therefore hypothesized that *in vivo*-generated Th9 cells might undergo STAT-dependent bystander activation to promote airway inflammation. Because bystander activation was restricted to recently activated *in vitro*-Th9 cells, we first asked whether lung-resident Th9 cells had an activated phenotype. We compared transcriptomes of lung-resident IL-9^+ and IL-9^- $CD4^+CD44^+TCR\beta^+$ cells from INFER mice exposed to the chronic papain model of airway inflammation, which induces expansion of IL-9-producing T-cells and is attenuated in the absence of IL-9 (Fig 5a-h**, S5k-m, 6a-f, S6f-k**)[8,16,20]. We identified four activation-induced TFs for which we could generate target genesets using public data (TF deletion or overexpression): NFAT, IRF4, JunB, and NF-κB. We compared net enrichment of TF-induced genes in Th9 vs. non-Th9 cells (GSEA), using STAT-target genesets as controls (Fig 5a). As a positive control, Th9 cells showed increased net expression of STAT6-induced genes. Lung-resident Th9 cells were also enriched for activation-dependent TF targets (Fig 5a), indicating that they had an activated transcriptomic signature.

Pulmonary Th9 cells undergo bystander activation *in vivo*

Having determined that lung-resident Th9 cells from papain-treated mice have an activated signature, we next assessed for evidence of bystander activation *in vivo*. To block TCR-activation, mice were treated between papain sensitization and challenge

with an antibody against major histocompatibility complex class II (αMHCII) that was previously shown to prevent TCR-activation in the airway (Fig 5b)[43]. αMHCII-treated mice developed peribronchial leukocyte infiltration, goblet hyperplasia, and mucus production indistinguishable from isotype-treated mice. In lung-resident $CD4^+$ T cells, αMHCII had no effect on expression of IL-9 or other effector cytokines (Fig 5c-e**, S5a-c**). These findings demonstrate that Th9 cells and Th2 cells can undergo MHCII/TCR-independent activation and tissue infiltration *in vivo*.

We next sought to confirm TCR-independent activation of differentiated Th9 cells using a genetic approach. The Tec family kinase Itk is required for full TCR signaling and is critical for Th9 differentiation; we confirmed this by differentiating Th9 cells *in vitro* in the presence of a pharmacologic Itk inhibitor (**Fig S5d**)[20]. We hypothesized that Itk signaling was dispensable for restimulation of Th9 cells *in vitro* and *in vivo*. Pharmacologic Itk inhibition did not affect IL-9 production from *in vitro* differentiated Th9 cells; as a positive control, inhibition reduced TCR-stimulated IL-4 production from Th2 cells (**Fig S5e-f**). To study acute TCR-Itk signaling *in vivo*, we crossed mice bearing exon 3 of *Itk* flanked by two loxP sites with mice expressing ERT-Cre to generate Itk^{ERT} mice (**Fig S5g**). We confirmed that deletion of Itk inhibited *in vitro* Th9 differentiation, recapitulating germline Itk deficiency (**Fig S5h**). To determine whether *in vivo* ablation of TCR-Itk signaling affected Th9 reactivation after *in vivo* differentiation of Th9 cells, mice were treated with tamoxifen for 5 days between papain sensitization and challenge, to delete exon 3 of *Itk* in $CD4^+$ and $CD8^+$ T cells (**Fig S5i-j**). Itk ablation had no significant effect on lung pathology or IL-9- and IL-13-producing pulmonary $CD4^+$ T cells (**Fig S5k-n**), confirming that tissue-infiltrating Th9 cells can undergo TCR-independent activation *in vivo*.

While Th9 cells are important drivers of airway inflammation *in vivo*, type 2 innate lymphoid cells (ILC2) also induce lung pathology by producing type 2 cytokines independent of antigenic stimulation[8,38]. To eliminate this confounding factor, we treated ILC2-deficient ($Gata3^{\Delta KLRG1}$) mice with αMHCII between papain-sensitization and challenge (Fig 5a). Treatment with papain induced IL-9 in $CD4^+$ T cells but had no effect on IL-9 production in other cell types (Figure 5f-h**, S5o**). Although airway inflammation was attenuated in ILC2-deficient mice, αMHCII had no significant effect on airway pathology, IL-9-producing pulmonary $CD4^+$ T cells, or IL-13-producing $CD4^+$ T cells (Fig 5f-h**, S5p-r**). This established that TCR-independent restimulation was sufficient to induce pulmonary Th9 infiltration, Th9 activation, and allergic lung pathology, even in the absence of ILC2.

Bystander Th9 activation promotes airway inflammation *in vivo*

Although Th9 cells are important mediators of papain-induced airway inflammation, other cell types like eosinophils and mast cells can also produce IL-9, while other cytokines like IL-13 and IL-17A can promote airway inflammation. We therefore used a Th9-specific model to determine whether STAT-dependent activation of Th9 cells induces airway inflammation. We differentiated ovalbumin (OVA)-specific (OT-II) Th9 cells from INFER mice *in vitro*, transferred sorted-GFP^+ ($IL\text{-}9^+$) $CD4^+$ cells into congenic hosts, and rechallenged recipient mice with intranasal IL-2 + IL-4 (**Fig S6a**). This promoted lung inflammation and induced IL-9 production from donor OT-II Th9 cells, revealing that Th9

cells can induce *in vivo* pathology in the absence of cognate antigen if they are stimulated with IL-2 + IL-4 (Fig 6a-c). Thus, STAT5- and STAT6-dependent Th9 bystander activation can promote airway inflammation *in vivo*, in the absence of acute MHC-II/antigen-TCR interactions.

Th9 expansion correlates with responsiveness to JAK inhibitors

The importance of STAT-dependent bystander activation to Th9 effector function suggested that JAK-STAT inhibitors (jakinibs), which are efficacious for allergic diseases[32], might prevent acute Th9-driven pathology. We therefore treated C57BL/6 mice with the pan-jakinib tofacitinib to block JAK-STAT signaling between papain sensitization and challenge (**Fig S6b**). Tofacitinib-treated mice had significantly less peribronchial leukocyte infiltration, goblet hyperplasia, and mucus production than vehicle-treated mice (Fig 6d-e). In pulmonary $CD4^+$ T cells, tofacitinib significantly reduced production of IL-9 but not of other cytokines (Fig 6f**, S6c-e**,. Tofacitinib did not affect airway inflammation in mice treated with IL-9-blocking antibodies (**Fig S6f-k**). Together, these findings suggest that blocking Th9 activation with JAK-STAT inhibitors could ameliorate allergic disease flares.

This led us to hypothesize that peripheral Th9 expansion, which can be seen in allergic patients (Fig 2h**, S2f**) and is associated with STAT5 activation[36], might correlate with responsiveness to jakinibs. We therefore analyzed transcriptomes of HDM-treated $CD4^+$ T cells from allergic patients, which had high *IL9* and "allergic Th9" gene expression (Fig 6g**, S3j**)[16]. STAT5- and STAT6- induced genes were enriched in allergic $CD4^+$ T cells relative to healthy volunteer cells (GSEA, Fig 6g). Moreover, STAT5- and STAT6- induced genes were enriched in allergic cells with high *IL9* expression (> mean expression, Fig 6h) relative to cells with low *IL9* expression (< mean expression, Fig 6h). In a separate dataset (GSE6281), nickel-allergic patients were exposed to nickel for 96 hours, inducing inflammation, *IL9* expression (**Fig S6l**), and STAT5- and STAT6-target genes (**Fig S6m-p**). This suggested that Th9 cells from allergic patients are poised to respond to jakinibs, and that Th9 expansion might be associated with jakinib-responsiveness. We therefore investigated skin transcriptomes of atopic dermatitis patients with enriched "allergic Th9" genes (**Fig S3j**), in whom *IL9* expression correlated with response to a JAK-SYK inhibitor[44]. Expression of STAT5- and STAT6- induced genes decreased in post-treatment lesional skin relative to pre-treatment skin (Fig 6i). Hence, in patients with allergic disease, Th9 expansion is associated with STAT5 activation, STAT6 activation, and responsiveness to jakinibs. This suggests that Th9 expansion may predict a jakinib-responsive endotype, further increasing the relevance of STAT-dependent Th9 bystander activation to human allergic disease.

Discussion

Th9 cells are critical inducers of allergy, autoimmunity, and antitumor immunity[6,7,11,12,14,45]. However, major questions surround the regulation and function of Th9 cells. These include the mechanisms underlying transient dynamics of IL-9 production, the physiological significance of Th9 lineage instability, and the molecular mechanisms regulating human Th9 effector function in patients with inflammatory diseases. Herein, we

addressed these questions using genetic and functional approaches in human primary cells and murine models.

STAT5 and STAT6 are both critical for Th9 differentiation[24-26,37]. Here, we provide evidence that IL-9 is also induced by STAT5- and STAT6- dependent bystander activation, indicating a broader role for these TFs in Th9 effector function. This mechanism is unique to Th9 cells: Th1, Th2, and Th17 bystander activation are induced by IL-1 family members, although STATs can enhance NF-κB-dependent activation[30]. Moreover, Th1, Th2, and Th17 bystander activation requires prolonged stimulation whereas Th9-bystander activation is rapid[30]. The reasons for these Th9-specific mechanisms and kinetics may be related to the role of Th9 cells in anti-helminth immunity, where antigen-specific responses are suppressed[29]. While antigen-independent IL-9 production can also derive from non-T-cell sources like ILC2 and mast cells, Th9 cells serve important nonredundant functions because of their capacity for circulation, plasticity, and expansion[40,42,46]. Bystander activation may also promote Th9 function in immune-privileged sites like the central nervous system and tumor microenvironment[45,47,48]. The transient kinetics of bystander activation may constrain prolonged nonspecific Th9-mediated inflammation. The responsiveness of circulating IL-9-producing T cells from allergic patients – but not healthy volunteers – to STAT-dependent cytokines suggests that this negative checkpoint breaks down in allergic disease. This could promote Th9 stability in allergic patients, suggesting a novel potential driver and therapeutic target.

In addition to providing major insights about Th9 effector function, this mechanism of bystander activation is also translationally useful. Th9 expansion is associated with STAT5- and STAT6- induction and responsiveness to jakinibs in murine models and allergic patients. This suggests that Th9 expansion might be a biomarker for a jakinib-responsive endotype. Moreover, adding IL-2 and IL-4 to TCR mimetics improves detection of rare circulating human IL-9$^+$ cells, and therefore of patients with Th9-expansion. Thus, STAT-dependent Th9 bystander activation not only defines a druggable allergic endotype but can also be leveraged to detect patients with this endotype. Further studies can determine how peripheral Th9/IL-9 induction can be used to best target biologic therapies for patients with allergic diseases.

Our findings also advance the understanding of Th9 identity. Previous studies have yielded conflicting results about the identity of the “Th9” subset, possibly due to disease- and tissue-specific differences in IL-9$^+$ T cells. We resolve several of these questions using a transcriptional program of IL-9$^+$ T cells developed using multiple independent datasets. While overlap of DEGs from individual datasets was low, net expression of this cassette was enriched in several additional independent datasets obtained from *IL9*$^+$ allergic subjects, indicating that this cassette is characteristic of “allergic Th9” cells. Enrichment of the “allergic Th9” cassette in antitumor Th9 cells also demonstrates a conserved identity for IL-9$^+$-T cells in different immunological contexts. Enrichment of “allergic Th9” genes in *in vitro*-generated Th9 cells, indicates that these cells are an appropriate model to study Th9 lineage identity. Within the “allergic Th9” cassette, co-expression of genes encoding conventional Th2 cytokines, activation markers, Granzyme B, and GM-CSF suggests that Th9 cells are a distinct group of highly activated cells that produce a unique

combination of proinflammatory cytokines. Analysis of the “allergic Th9” cassette indicates responsiveness to antiviral cytokines like TL1A and to IL-1β, which potentiates IL-2/STAT5 signaling during Th9 differentiation and enhances the differentiation of “inflammatory Th2” cells[21,31,49]. Both cytokines are elevated during allergic inflammation and could promote Th9 activation, enhancing bystander IL-9 induction. Finally, following “allergic Th9” gene expression over time suggests that Th9 cells do not simply differentiate into conventional Th2 cells but rather maintain a distinct inflammatory phenotype.

Apart from the transcriptome, Th9 identity can also be studied by profiling the epigenome, including human *IL9* locus structure and regulation. Th9 cells are regulated by a broad network of TFs including PU.1/ETV5, GATA3, STATs, TAK1, and RARα that directly target the *Il9* locus[13,16,17,19,25,27]. These mechanisms have largely been investigated in mice, yet there are fundamental differences in human and murine Th9/IL-9 regulation. By integrating human and murine data, our work provides a highly translational model of *IL9* regulation that identifies and utilizes the most relevant murine models of human Th9/IL-9 biology. For example, we find that *IL9* regulation correlates with Th2 locus regulation in human Th9 cells more closely than murine cells. This may relate to fundamental differences in chromatin structure: human *IL9* is located 3kb from the Th2 locus whereas the murine *Il9* and Th2 loci are on different chromosomes. Hence, it may be necessary to study *IL9*-associated topologically associated domains (TADs), Th2 locus interactions, and long-range interactions primarily in human cells. Combining transcriptomic and epigenomic data reveals dynamic STAT5-target induction and STAT1-target repression in murine and human cells, but inconsistent results for STAT3. This is consistent with reports that STAT3 represses murine Th9 development by restraining STAT5 while promoting human Th9 differentiation by restraining STAT1[35,37]. Our findings suggest that future investigations of STAT5-STAT1 interactions may resolve some of these inconsistencies.

Our epigenetic data also uncover a novel mechanism underlying the unstable Th9 phenotype. In murine and human cells, the *Il9/IL9* locus gains accessibility during differentiation, permitting effector function. However, critical cis-REs close over time, rendering *Il9/IL9* refractory to transcriptional induction. Because T effector function depends on the chromatin state of cytokine loci[50], these epigenetic changes prevent Th9 lineage commitment. The transient nature of changes is more pronounced in murine Th9 cells than in human cells, and circulating IL-9^+ memory T cells are reliably identified in allergic patients but not in healthy volunteers. The determinants of human Th9 stability will require further studies using cells from subjects with IL-9-associated diseases. Because Th9 cells are implicated in a broad cross-spectrum of diseases, studying human Th9 in diverse cohorts should uncover factors promoting lineage commitment in the context of these varied pathologies.

In summary, post-differentiation murine and human Th9 cells become transiently susceptible to TCR-independent, STAT-dependent bystander activation upon stimulation with IL-2 and IL-4. This mechanism is restricted to recently activated cells because of dynamic *Il9/IL9* locus remodeling. Epigenetic changes reduce accessibility of STAT5-binding sites, rendering *Il9/IL9* refractory to transcriptional induction and causing Th9 instability. Finally, STAT-dependent activation promotes TCR-independent Th9-mediated pathology *in vivo* and is

associated with responsiveness to jakinibs in patients with Th9-expansion. These results not only advance our understanding of the basic mechanisms of allergic inflammation and T helper lineage commitment, but also define a novel potential allergic endotype.

Methods

Human samples

De-identified buffy coats for healthy volunteers were obtained from the National Institutes of Health Blood Bank. Whole blood was obtained from idiopathic atopic dermatitis (AD) patients who were evaluated at NIH Clinical Center under the IRB-approved protocol NCT01164241. Human tonsil samples from noninflamed volunteers with sleep-disordered breathing were obtained from Children's National Hospital in Washington, DC under a multi-site IRB-approved protocol in which NIH was the IRB of record (94-HG-0105). All subjects provided written informed consent, and all experiments were done with male and female subjects. Subjects were not compensated.

Animal experiments

Experiments were done on 8-14-week-old mice that were age- and sex- matched within experiments. All experiments were done in male and female mice and were performed in an AAALAC-accredited animal facility, approved by the NIAID Institutional Animal Care and Use Committee, in accordance with NIH guidelines for the use and care of live animals, under protocol LAD12E. Mice were maintained in a specific pathogen free facility on a 12h light/dark cycle, in open cages with food and water continuously available. Mice were checked periodically to ensure normal health and more often if adverse effects were anticipated. All mice were on a C57BL/6 background. *Gata3*$^{fl/fl}$ and *ERT*^{Cre} mice were purchased from Jackson. *Cd45.1 x Rag*$^{-/-}$ *x OT-ii* mice were purchased from Taconic. INFER and *Klrg1*^{Cre51} mice were generously provided by Drs. Richard Flavell and Paola Licona-Limon. ILC2-deficient mice were generated by crossing *Klrg1*^{Cre} to *Gata3*$^{fl/fl}$ mice[52]. Detailed characterization of ILC2-deficient mice has been reported[53].

To generate *Itk*^{ERT} mice, two loxP sites flanking exon 3 of *Itk* were introduced into the genome. A targeting vector (pL253) containing exon 3 flanked by two LoxP sites was generated by recombineering[54]; a neomycin resistance gene (Neo) flanked by two FRT sites was inserted before the second LoxP site for drug selection. The vector was linearized and electroporated into HGTC-8 ES cells; genomic DNA was isolated from G418-resistant cell clones and screened by long-range PCR. Correct integration of targeted ES clones was confirmed by Southern blots, and successfully targeted ES clones were microinjected into C57BL/6 blastocysts. Germline transmission from generated chimeric offspring was confirmed by genotyping. Mice carrying the targeted allele were bred to Flp recombinase transgenic mice (NHGRI Transgenic Core) to remove the FRT-flanked Neo cassette and to generate *Itk*$^{fl/fl}$ mice. To delete *Itk*, *Itk*$^{fl/fl}$ mice were bred to B6(129S4)-Et(cre/ERT2)6691Rdav/J (Jackson), which express the tamoxifen-inducible Cre-ERT2 fusion protein (Cre-ER^{T2}). Genomic DNA was genotyped by PCR (gen Itk in3 F: 5' TGCTTACTCTAGGAGAACAAGG 3', gen Itk in3 R: 5' GCTACTTAGACAATTGGAGGC

3') which generated a 600 bp band from the wild type allele, a 785 bp band from the floxed allele and a 342 bp band from the knockout allele.

Reagents

All recombinant cytokines were obtained from Peprotech except for hIL-12, mIL-12, TSLP, GM-CSF, TL1-A, and hTGF-β (R&D). Details of antibody clones and validation are provided in Source Data. Tofacitinib, FK506, BAY11, CAY10571, STAT5-INHIBITOR, and STAT6 inhibitor AS1517499 were purchased from Cayman and reconstituted in DMSO to 100 mM, 10 mM, 50 μM, 100 mM, 50 μM, and 50 nM stock concentrations, respectively.

In vitro human T cell differentiation

Human peripheral blood mononuclear cells (PBMC) were isolated by density centrifugation (Ficoll-Paque). Naïve human $CD4^+$ T cells were magnetically enriched to >95% purity (StemCell) and plated at a density of 0.5 $x10^6$ in 1 mL in a 24-well plate for Th1 and Th2 differentiation, and 1 $x10^6$ in 2 mL in a 24-well plate for Th9 differentiation on plate-bound αCD3 (1 μg/mL, OKT3). Cells were cultured in complete RPMI-1640 with glutamine (10% FBS, 100 IU/mL penicillin, 0.1 mg/mL streptomycin) in the presence of cytokines and antibodies to promote the differentiation of Th1 (1 μg/mL αCD28; 2.5 μg/mL αIL-4; 10 ng/mL hIL-12, 1 ng/mL hIL-2); Th2 (1 μg/mL αCD28, 2.5 μg/mL αIFN-γ, 2.5 μg/mL αIL-10, 30 ng/mL hIL-4, 10 ng/mL hIL-2), Th9 (1 μg/mL αCD28, 2.5 μg/mL αIFN-γ, 5 ng/mL hTGFβ, 10 ng/mL hIL-2, 30 ng/mL hIL-4, 10 ng/mL hIL-1β. For supernatant collection experiments, Th1 and Th9 cells were cultured for 5 days and Th2 cells were cultured for 9 days prior to restimulation. For all other experiments, after 5 days cells were washed and cultured without αCD3 or αCD28 but with all polarizing cytokines and antibodies for an additional 3-15 days (media, cytokines, and antibodies changed every 2 days). Cells were collected on day 5-20 for stimulation and analysis; resting cells were defined as cells not being cultured on αCD3 or αCD28 (days 6 and onward).

In vitro mouse T cell differentiation

Murine naïve $CD4^+CD62L^+$ cells were isolated from spleen and lymph nodes using negative selection (Miltenyi) followed by flow sorting to >95% purity. Cells were cultured in complete IMDM (10% FBS, 100 IU/mL penicillin, 0.1 mg/mL streptomycin, 55 μM 2-Mercaptoethanol) at a density of 0.5 $x10^6$ in 1mL in a 24 well plate for Th1, Th2, and Th9 differentiation. Cells were activated with plate bound αCD3Ɛ (10 μg/mL) and αCD28 (10 μg/mL) for 3 days with polarizing cytokine and antibodies to promote the differentiation of Th1 (10 μg/mL αIL-4, 10 ng/mL mIL-12,), Th2 (10 μg/mL αIFN-γ, 20 ng/mL mIL-4), Th9 (10 μg/mL αIFN-γ, 20 ng/mL mIL-4, 10 ng/mL hIL-2, 5 ng/mL hTGF-β). After 3 days, cells were washed and cultured without αCD3 or αCD28 but with polarizing cytokines and antibodies, and with 10 ng/mL hIL-2, in fresh media. Media, cytokines, and antibodies were changed every 2 days. Cells were collected on day 3-10 for stimulation and analysis; resting cells were defined as cells not being cultured on αCD3 or αCD28 (days 4 and onward).

For Itk inhibitor experiments, $CD4^+$ T cells were purified by magnetic cell separation (Miltenyi) from pooled lymph nodes and spleens. Naive $CD4^+$ T cells ($1.2\text{-}2 \times 10^5$) were co-cultured in complete IMDM media, at a ratio of 1:5 with mitomycin C treated T-depleted

splenocytes as APCs in 48-well plates under Th9 conditions (1μg/ml αCD3, 3μg/ml αCD28, 30ng/ml IL-4, 7.5ng/ml TGFβ1, 15ng/ml mTL1A, 15μg/ml αIFN-γ, 15μg/ml αIL-12) or Th2 conditions (1μg/ml αCD3, 3μg/ml αCD28, 60ng/ml IL-4, 30μg/ml αIL-12) for 3 days[20]. In some experiments Itk inhibitor (BMS 509744) was used at the indicated concentrations, either during T helper differentiation or during restimulation. In some experiments, mice were treated with intraperitoneal tamoxifen 100 μg IP daily for 4 days before isolation of naïve T cells, to delete *Itk*.

Restimulation

All cells were stimulated in 96-well plates. For *ex vivo* stimulations, PBMC from AD patients, PBMC from healthy volunteers, and tonsil samples were thawed and washed x2 with complete RPMI-1640 with 10 U/mL DNase I (Roche). PBMCs and tonsil cells were stimulated with 20 ng/mL hIL-2; 40 ng/mL mIL-4 for 2h, followed by brefeldin A (10 μg/mL) for 4h (total 6h) at 37°C. *In vitro* differentiated T cells, cells were washed x3 prior to restimulation. For supernatant collection experiments, Th1, Th2, and Th9 cells were stimulated in fresh media with plate-bound αCD3 for 48h. For other experiments, murine T cells were stimulated with the following agents alone or in combination, as detailed in individual experiments: 100 ng/mL phorbol 12-myristate 13-acete (PMA, Calbiochem); 1 mg/mL ionomycin (Sigma); 20 ng/mL hIL-2; 40 ng/mL mIL-4. Human T cells were stimulated with (alone or in combination) 20 ng/mL PMA; 1 mg/mL ionomycin; 20 ng/mL hIL-2; 60 ng/mL hIL-4. In some experiments, cells were stimulated with escalating doses of IL-2 and IL-4 as indicated. In some experiments, cells were stimulated with escalating doses of plate bound αCD3 as indicated. In some experiments, cells were restimulated with 30 ng/mL IL-9, 10 μg/mL LIGHT, 10 μg/mL ICOS, 10 μg/mL H7-2, 200 ng/mL OX40L, 10 ng/mL hIL-12 , 100 ng/mL hIL-21, 50 ng/mL IL-7, 10 ng/mL IL-6, 100 ng/mL IL-1β, 50 ng/mL TSLP, 100 ng/mL TL1-A, 100 ng/mL IL-18, 100 ng/mL IL-17A, 100 ng/mL IL-33, 100 ng/mL IL-36α, 100 ng/mL IL-36γ, or 100 ng/mL GM-CSF. For flow cytometric measurement of intracellular cytokines, cells were treated with brefeldin A (10 μg/mL) after 1.5 hours and stimulated for an additional 4.5h (6h total) at 37 °C. In some experiments, cells were treated with tofacitinib (0.3 μM), FK506 (10 nM), BAY11 (5 μM), CAY10571 (25 μM), STAT5-INHIBITOR (Cayman, CAS 285986-31-4, 50 μM), or the STAT6 inhibitor AS1517499 (Cayman, 50 nM) for 20 min before restimulation or during differentiation as indicated.

For supernatant-stimulation experiments, d8 human Th9 cells were washed and resuspended in 200 μL of supernatants for up to 6 hours. Brefeldin was added after 2 hours. In some experiments the following antibodies were added at 20 μg/mL: isotype, αIL-2, αIL-4, or αIL-1β.

For Itk inhibitor experiments, *in vitro* differentiated cells were stimulated for 4h with plate bound αCD3(1ug/ml) + αCD28(3ug/ml) in presence of Golgistop (BD) in absence or presence of 1μM or 500 nM Itk inhibitor (BMS-509744, Calbiochem).

For pulmonary T cell analysis, cells were stimulated with PMA (100 ng/mL), Ionomycin (1mg/mL), hIL-2 (20 ng/mL) and mIL-4 (40 ng/mL) for 2h followed by brefeldin A (10 μg/mL) for 3h (total 5h) at 37°C.

Flow cytometry

I*n vitro* differentiated cells were stained with Zombie Aqua™ dye (BioLegend) for 15min in 4 °C, then fixed with Cytofix/Cytoperm (BD Bioscience) and underwent intracellular staining. For Itk inhibitor experiments, *in vitro* differentiated Th9 cells underwent surface staining for CD4 prior to fixation. For phospho-STAT staining, after viability staining cells were fixed with 1.6% PFA for 10 min in dark at RT then treated with ice-cold methanol overnight at −20 °C. Cells were washed with FACS buffer and intracellular staining antibodies were added. Cells isolated from lung tissue were stained with Zombie Aqua for 10 min in the presence of mouse Fc block (20 μg/ml, BioXCell, #BE0307), rat serum (1:50, ThermoFisher, #10710C), hamster serum (1:50, Abcam, #ab7483). After 10 minutes, surface staining antibodies were added for 20 minutes. Cells were then fixed (BD Cytofix/Cytoperm) and stained with intracellular antibodies in the presence of Fc block.

The following antibodies were used for intracellular staining of human cells (full panels available in Source Data): Human Fc block/IgG (10 μg/ml, MP Biomedicals, LLC, #82310) , CD3 APC-Cy7 (SK7) or CD3 AF700 (UCHT1), CD4 BUV395 (RPA-T4), CD8 APC-Cy7 (SK1), CD45RO PE-Texas-red (ECD), IL-2 PerCp-Cy5.5 (MQ1-17H12), IL-4 FITC or BV605 or PE-Cy7 (MP4-25D2), IL-5 BV421 (TRFK5), IL-9 PE (MH9A4), IL-10 PE-Cy7 (JES3-9D7), IL-13 BV711 (JES 10-5A2), IL-17A APC (ebio64CAP17), IFNγ AF700 or V450 (B27), p Y694-STAT5 v450 (47), pY641-STAT6 PerCp-Cy5.5 (18-1P-stat6). The following antibodies were used for murine cells (full panels available in Source Data): CD45.1 PerCp-Cy5.5 (A20), CD45.2 FITC or PE-Cy7 (104), CD44 AF700 (IM7), TCRβ APC-Cy7 (H57-597), CD4 PerCP-Cy5.5 (RM4-5) or CD4 V450 or BUV737 (GK1.5), IL-2 PE-Cy7 (MQ1-17H12) or IL-2 PE (JES-6-5H4), IL-4 PE-Texas-red or AF488 (11B11), IL-9 APC or PE or BV421 (RM9A4), IL-13 V450 or PE-Cy7 (eBio13A), IL-17A FITC (TC11-18H10.1), IFNγ PE or BV605 (XMG1.2).

Data were collected on an LSR Fortessa (BD Biosciences) or FACS Symphony A5-4 (BD Biosciences) and analyzed with FlowJo (Treestar). Gating strategies for murine experiments are shown in **Figure S7**, and gating strategies for human experiments are shown in **Figure S8**.

Cell sorting

Human naïve $CD4^+$ T cells were enriched by magnetic separation (StemCell), then stained with Zombie Aqua, CD19 AF488 (HIB19), CD16 FITC (3G8), CD14 FITC (M5E2), CD4 APC (S3.5), CD8 APC-Cy7 (SK1), CD45RA BV711 (HI100). $Aqua^-/CD4^+/CD45RA^+/CD19^-/CD16^-/CD14^-$ cells were sorted on a FACS Aria. For ATAC-seq experiments, *in vitro* differentiated Th9 cells were stained with DAPI and CD45RO PE-Texas-red and sorted for $DAPI^-/CD45RO^+$ cells.

Mouse naïve $CD4^+$ T cells were enriched using magnetic separation (Miltenyi), then stained with DAPI, CD62L PE-Cy7 (MEL-14), CD25 PE (PC 61.5), CD4 V450 (GK1.5), and CD44 AF700 (IM7). $DAPI^-/CD4^+/CD25^-/CD44^{lo}/CD62L^{hi}$ cells were sorted on a FACS Aria. For ATAC-seq experiments, *in vitro* differentiated Th9 cells were stained with DAPI and sorted

for DAPI$^-$ cells. For plasticity experiments (Fig 3), d3 Th9 cells from INFER mice were stained with DAPI, and DAPI$^-$/GFP$^+$ cells were sorted on a FACS Aria.

Papain induced Asthma

All *in vivo* studies were randomized. Mice were anesthetized with isoflurane and exposed intranasally (IN) to 25 μg papain (Calbiochem) in 30 μl PBS on day 0, 3, 6, and 13. 10-12 hours after the last IN injection, mice were euthanized. In some experiments, 100 μg αMHC2 (clone Y-3P) or isotype (BioXCell) were administered daily by intraperitoneal injection (IP) on day 12 and 13. We validated activity of this antibody *in vivo* (see below). In some experiments, 50 mg/kg tofacitinib in 0.5% methylcellulose was administered twice daily IP on day 12 and 13. In some experiments, mice were treated with 100 μg αIL-9 (clone 9C1) or isotype antibody (BioXCell) every other day by intraperitoneal injection (IP) on day 0-14. For *Itk* deletion experiments, Mice were anesthetized with isoflurane and exposed intranasally (IN) to 25 μg papain (Calbiochem) in 30 μl PBS on day 0, 3, 6, 14, and 21, then euthanized 10-12 hours after the last IN injection as above. On days 10-14, mice were treated with tamoxifen 100 μg IP daily. After euthanasia, lung tissues were fixed in 10% neutral buffered formalin solution. Paraffin embedded sections (5 μm) were stained with hematoxylin and eosin (H&E) or Periodic Acid-Schiff (PAS). Cells from lung were isolated and digested in collagenase Type IV (100 unit/mL; Gibco) for 70 min at 37 °C. After digestion, cells were lysed with ACK buffer (Gibco) for 30-60 sec and strained through a 40 μM strainer, then stimulated and stained as above.

Th9 Adoptive Transfer and OVA asthma

All *in vivo* studies were randomized. To validate αMHC2 *in vivo*, mice were exposed IP ovalbumin (OVA) on day 0 and 7, followed by IN OVA on day 15 and 16. 100 μg αMHC2 (clone Y-3P) was administered IP on day 15 and 16, and mice were euthanized on day 18. To generate ovalbumin (OVA)-specific Th9 cells, INFER (GFP IL-9 reporter) mice were crossed to Rag2$^{-/-}$ OT-II CD45.1$^+$ mice. Resulting INFER/Rag2$^{-/-}$ OT-II CD45.1$^+$ CD45.2$^+$ naïve T cells were co-cultured with antigen presenting cells (APCs) under Th9 promoting conditions as previously described[16]. On day 3, cells were collected and stained with Zombie Aqua and antibodies to CD4, CD45.1, and OT-ii as above. IL-9$^+$ Th9 cells were sorted (DAPI$^-$/CD4$^+$/OT-ii$^+$/CD45.1$^+$/GFP$^+$) and washed x3 with PBS. 1x10^6 Th9 cells were injected retroorbitally into congenic (CD45.2) C57BL/6 mice. After 24h, mice were anesthetized as previously described[16] and exposed intratracheally to mIL-2 (100 ng) and mIL-4 (500 ng). After 48h, mice were anaesthetized with isoflurane, challenged intranasally with mIL-2 (100 ng) and mIL-4 (500 ng), and euthanized 12h after the last challenge.

Scoring Papain induced asthma and OVA-asthma

Lung histology was scored blindly by a pathologist as previously described based on perivascular cuffing, peribronchial cuffing, interstitial inflammation, and goblet cell hyperplasia[16].

Enzyme-linked immunosorbent assay (ELISA)

ELISA for human IL-2 (BioLegend), IL-4 (BioLegend), and IL-9 (R&D system) were performed according to the manufacturer's protocol. Absorbance readings (450 nm and 570 nm) were collected on a TECAN plate reader.

mRNA extraction and reverse transcription quantitative PCR (RT-qPCR)

Cells were suspended in Trizol LS (Invitrogen), and total RNA extracted according to the manufacturer instruction. 250 ng RNA was reverse transcribed using cDNA synthesis kit (Applied Biosystems™) and qPCR performed in triplicate using TaqMan master mix (Applied Biosystems™) and primers for *IL9* (Hs00174125_m1) and 18S (Hs99999901_s1). Fold change in transcript level was calculated by normalizing threshold values to 18S.

Nascent RNA extraction and digital droplet PCR (ddPCR)

To measure nascent RNA level in human Th9 cells, total RNA was extracted as above. EU-labeled cellular RNAs were separated using the Click-it Nascent RNA Capture kit (ThermoFisher) according to the manufacturer's protocol. Nascent *IL9* expression was measured relative to *TBP* (BioRad cat 10031257).

RNA-seq library preparation

mRNA was extracted as above. Libraries for mRNA-sequencing were prepared using the NEBNext Ultra II Directional RNAseq Library kit, per the manufacturer's instructions. Samples were sequenced on a NovaSeq 6000, paired end, 50 cycles, and processed with bcl2fastq v2.20.0.422.

RNAseq analysis

Reads of 50 bases were processed using the rna-seek pipeline (https://ccbr.github.io/RNA-seek/). Briefly, adapter sequences were trimmed with cutadapt 1.18 and mapped to the mouse transcriptome and genome mm10 or human transcriptome and genome GRCh38 (hg38) using STAR. Gene expression values (FPKM: Fragments Per Kilobase exon Per Million mapped reads; TPM, Tags Per Million mapped reads; counts) were generated using RSEM. Differential gene expression was calculated using DESeq2. To calculate fold-change cutoffs, datasets were normalized based on FPKM and purged of micro-RNAs, sno-RNAs and sca-RNAs. To minimize fold-change artifact from low abundance transcripts, a small offset was added to all RPKM values (0.37; equal to the averaged second quartiles of each dataset). When multiple transcripts were detected for one gene, only the most abundant (highest average RPKM across all replicates) was analyzed. Transcripts with FPKM < 1 were excluded. Downstream analyses were performed with R 4.2.2, Morpheus (https://software.broadinstitute.org/morpheus/), and DAVID (https://david.ncifcrf.gov/).

ChIP-seq sample and library preparation

ChIP-seq sample preparation was performed with Covaris kit (PN 520154) as previously described[16]. Naïve T cells were cultured *in vitro* under Th9 promoting conditions and treated with chemical cross-linking (1% formaldehyde) on days 0, 3, 4, and 8 (murine) or days 0, 5, 8, and 15 (human). At least 0.5 million cells were used for

each immunoprecipitation. After chemical chromatin cross-linking (1% formaldehyde), cells were washed and frozen at −80C. Cells were resuspended in Lysis Buffer B (Covaris) with protease inhibitors, and DNA fragmentation was performed on a Covaris Sonicator (ME220) for 8 min to an average length of 200-700 bp. After sonication, cells were immunoprecipitated with anti-H3K27Ac (ab4729; Abcam), anti-H3K4Me1 (ab8895; Abcam), and anti-H3K4Me3 (ab8580; Abcam). Genomic DNA (input) was prepared by treating aliquots of chromatin with proteinase K and heating to de-crosslink, followed by purification (28106, Qiagen). An aliquot of chromatin underwent immunoprecipitation, after which decrosslinking was performed. After recovering purified DNA, 5ng or more of DNA was used to generate libraries (NEBNext Ultra Directional II DNA sequencing kit). Samples were sequenced on a NovaSeq 6000, paired end, 50 cycles, and processed with bcl2fastq v2.20.0.422.

Chip-Seq analysis

Reads of 50 bases were processed using the ccbr pipeliner tool (https://ccbr.github.io/pipeliner-docs/). Briefly, adapter sequences were trimmed with cutadapt 1.18 and mapped to the mouse genome mm10, human genome hg19 (for bigwig files/visualization, to harmonize with ATAC-seq data), or human genome GRCh38 (hg38) (for peak calling) using BWAmem 0.7.17. Uniquely mapped and nonredundant reads were generated using Picard 2.17.11 and used for downstream analysis. The aligned files were converted to bam format using SAMtools 1.6, and bigwig files were created using deepTools 3.0.1. Genome browser files are displayed with IGV.

For downstream analysis, peaks were called using MACS v2.1.1 using FDR 0.01 and with the input sample for background correction. In the case of H3K4me1, H3K4me3, and H3K27Ac samples, "—broad" setting was used. Peaks were annotated using Uropa 4.2.1 and the annotatePeaks module in HOMER. Only regions called in both replicates were used in downstream analysis. After calling peaks with MACS, the union peaks of replicate samples were created using mergePeaks module in HOMER and divided into shared and dynamic peaks using the same utility. Motif enrichment analysis of dynamic peaks was done using the findMotifsGenome module in HOMER, *de novo* motif analysis.

ATAC-seq transposition and library preparation

Omni-ATAC-seq sample preparation was performed as previously described[55]. After flow cytometric sorting, 50,000 cells were lysed with 50 μl cold ATAC-Resuspension buffer (RSB) (10 mM Tris-HCl pH 7.4, 10 mM NaCl, 3 mM $MgCl_2$, 0.1% Tween 20) with 0.1% NP40, and 0.01% Digitonin on ice for 3 min. Lysis was stopped with 1 mL cold ATAC-RSB. After centrifugation (500×g for 10 min), nuclei were resuspended in 50μl transposition reaction containing 2.5μl Tn5 transposase (FC-121-1030; Illumina) to tag and fragmentalize accessible chromatin. The reaction was incubated at 37°C, 400rpm for 30 min; DNA was then purified using a MinElute kit (QIAGEN) and amplified with 8-12 cycles of PCR based on the amplification curve. Samples were purified using a MinElute kit, sequenced on a NovaSeq 6000, paired end, 50 cycles, and processed with bcl2fastq v2.20.0.422.

ATAC-sequencing

ATAC-seq reads from two biological replicates were used for each sample and analyzed as previously described[16]. Briefly, redundant paired end (PE) reads were removed using fastquniq. PE reads of 50 bases were aligned to the mouse genome build mm10 or human build hg19 with Bowtie 0.12.8, following the guidelines presented by Buenrostro et al[56]. Customized python scripts were used to calculate fragment length of each pair of uniquely mapped PE reads for size distribution analysis, and to group uniquely mapped reads into bins of 0 to 175 bases and 180 to 250 bases, respectively[38]. UCSC Genome Browser viewable and normalized BigWig files were generated with the Hypergeometric Optimization of Motif EnRichment program (HOMER) version 4.8. Genome browser files are displayed with IGV.

Only one mapped read to each unique region of the genome that was less than 175 bp was kept and used in peak calling. Regions of open chromatin were identified by MACS 1.4.2 using a p-value of 1×10^{-5}. Only regions called in both replicates were used in downstream analysis. Peak intensities ("tags" column) were normalized as tags per 10 million reads (RP10M) in the original library. Signal across all sites (i.e., all annotated genes and all accessible chromatin regions) was analyzed to eliminate potential bias by pre-selection. After calling ATAC-seq peaks with MACS, the union peaks of replicate samples were created using mergePeaks module in HOMER and divided into shared and dynamic peaks using the same utility.

Correlation analysis

For analysis of *Il9* and Th2 locus correlations (Fig S4g), chromatin accessibility and epigenetic marks, peaks were annotated based on proximity to the nearest gene and checked manually for *Il9/IL9*, *Il4/IL4*, *Rad50/RAD50*, *Il13/IL13*, and *Il5/IL5*. Tag densities (normalized reads) were calculated using HOMER. For each sample at each timepoint, the total number of tags at each gene locus were combined to obtain the total tag density over the entire locus. For RNA-seq data, FPKM-normalized gene expression for each gene was used. Pearson correlation values were calculated with R 4.2.2 for *Il9/IL9* with *Il4/IL4*, *Rad50/RAD50*, *Il13/IL13*, and *Il5/IL5*. Other downstream analysis and heatmap generation were performed as described above.

Selection and analysis of public gene expression datasets

For GSEA analysis[57,58], enrichment score curves and member ranks were generated by GSEA software (Broad Institute). For Figure 6, lists of TF-induced and TF-repressed genes were obtained using a previously published analysis of public datasets[16]. These included STAT1 (GSE40666), STAT3 (GSE65621); STAT4 (GSE40463); STAT5 (GSE77656); STAT6 (GSE40463), IRF4 (GSE39756); NF-kB[16]; NFAT (GSE64409); JunB (GSE98413). For Figures 3-6, public datasets were selected based on significantly increased *IL9* expression during allergic response as previously described or based on isolation and analysis of Th9 cells for datasets describing *in vivo* and *in vitro* generated Th9 cells[16]. The following datasets were selected: GSE97087, antitumor Th9 vs. Th1/Th17; GSE133385, lesional $IL9^{high}$ vs. nonlesional $IL9^{low}$ atopic dermatitis skin; GSE73482, house dust mite (HDM) stimulated T cells from allergic subjects vs. healthy volunteers; GSE133385, AD

patients treated with the JAK-SYK inhibitor ASN002; GSE146170, IL-9-expressing HDM-reactive T helper cells from allergic patients; MTAB-5739, IL-9-expressing T helper clones from healthy volunteers; GSE123501, in vitro differentiated Th9 cells and Th9 cells from IL-9-reporter mice treated with papain.

Additionally, the Gene Expression Omnibus was searched for datasets or series examining time-course gene expression in atopic or allergic inflammation, treated with JAK inhibitors and demonstrating significantly increased *IL9* expression during allergic response. Although no datasets were identified that detected *IL9* expression on transcriptome analysis, one dataset (GSE133385) was identified in which *IL9* expression measured by RT-qPCR increased during allergic response[44]. A list of public datasets used can be found in Extended Data Table 2.

For analysis of *ex vivo* human memory $CD4^+$ cell epigenetics, ENCODE tracks were analyzed directly in the igv browser [59].

Statistical analysis and reproducibility of PCR, flow cytometry, ELISA, and *in vivo* experiments

All *in vitro* experiments contained ≥ 3 biological replicates, and all data were expressed as mean ± SEM (bar/line graphs) or as min-to-max with lines at median (box plots). All *in vivo* experiments included 2-3 independent experiments with 1-6 animals per group per experiment, comprising ≥ 3 biological replicates. No statistical methods were used to pre-determine sample sizes but our sample sizes are similar to those reported in previous publications[7,16,18]. No animals/data points were excluded. Statistics were analyzed with GraphPad Prism 8.0. Normality testing was performed to determine whether samples were normally distributed. Normally distributed samples were analyzed using unpaired or paired Student's t-test. Nonparametrically distributed samples were analyzed using Wilcoxon test (paired) or Mann-Whitney test (unpaired). All statistical testing was 2-sided.

Extended Data

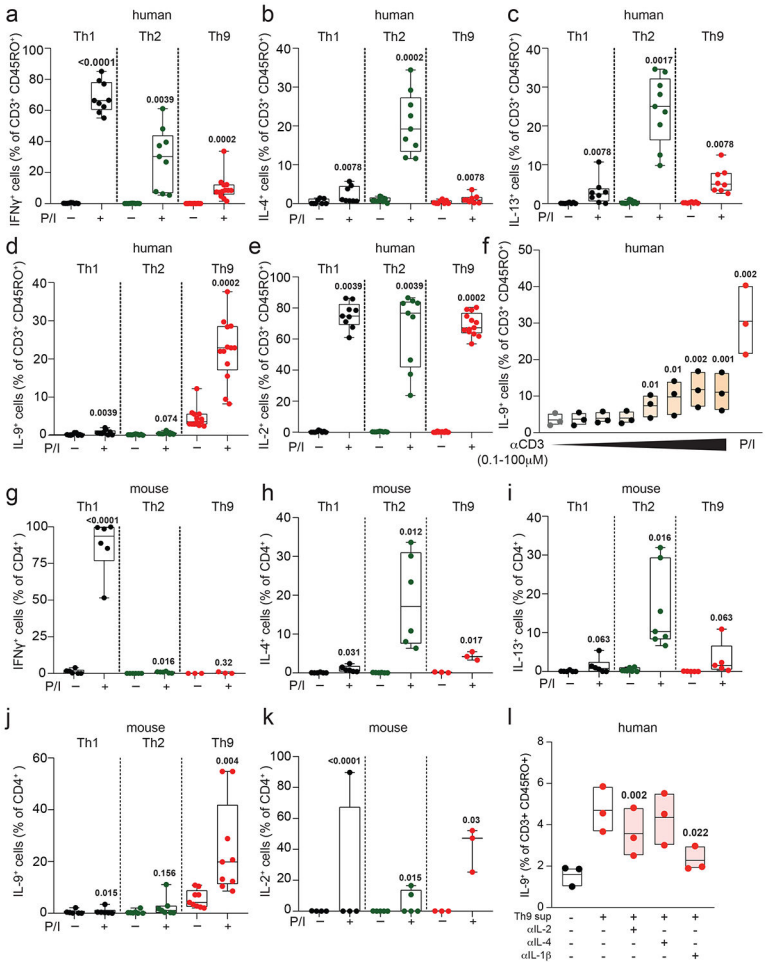

Extended Data Figure 1. Corresponds to Figure 1.

a-e. Naïve CD4$^+$ T cells from healthy volunteers were activated for 5 days with αCD3, αCD28, IL-2, and subset-promoting cytokines and antibodies. After 5 days, αCD3/αCD28 were withdrawn, and cells were cultured with IL-2 and subset-promoting cytokines and antibodies. Pooled results show production of IFN-γ (a), n=9 (Th1, Th2) or 10 (Th9); IL-4 (b), n=8 (Th1), 9 (Th2), or 4 (Th9); IL-13 (c) n=8 (Th1), 9 (Th2), or 4 (Th9); IL-9 (d) n=9 (Th1, Th2), or 10 (Th9); and IL-2 (e) n=9 (Th1, Th2), or 10 (Th9), with or without PMA and Ionomycin (P/I). **f.** Bar graphs show % IL-9 positive cells differentiated to d8 Th9 as above and restimulated with vehicle vs. plate bound αCD3 at escalating doses (n=3) **g-k.** Naïve CD4$^+$ T cells from WT C57BL/6 mice were activated for 3 days with αCD3, αCD28, IL-2, and subset-promoting cytokines and antibodies. After 3 days, αCD3/αCD28 were withdrawn, and cells were cultured with IL-2 and subset-promoting cytokines and antibodies. Pooled results show production of IFN-γ (f), n=6 (Th1, Th2) or 3 (Th9); IL-4 (g), n=6 (Th1, Th2) or 5 (Th9); IL-13 (h), n=6 (Th1), 7 (Th2), or 5 (Th9); IL-9 (i), n=6 (Th1), 7 (Th2), or 10 (Th9); and IL-2 (j), n=4 (Th1), 5 (Th2), or 3 (Th9), with or without P/I. **l.** Bar graphs show % IL-9$^+$ cells of resting (d8) human Th9 cells restimulated with Th9 supernatants and vehicle (n=3), αIL-2 (20 μg/mL), αIL-4 (20 μg/mL), or αIL-1β (20

μg/mL). For all line/bar graphs, error bars show ± S.E.M. Box plots show all data points (min to max, lines at median). For all experiments: paired or unpaired t-test, normally distributed data, Wilcoxon (paired) or Mann-Whitney (unpaired), non-normally distributed data. All statistical tests are 2-sided, all replicates are biologically independent samples.

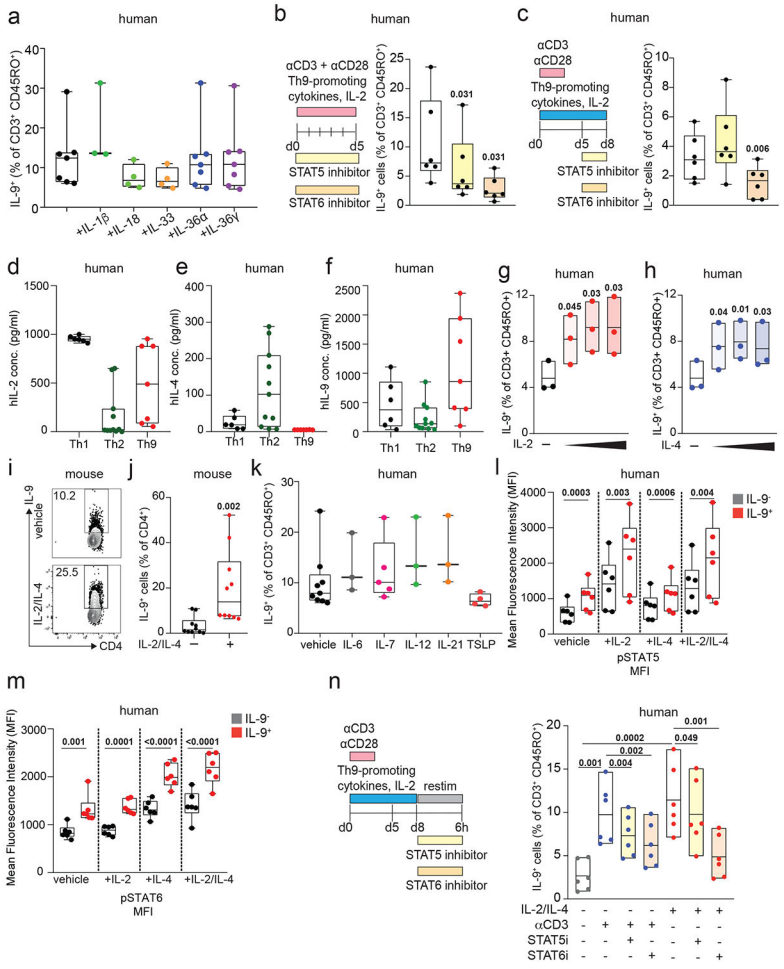

Extended Data Figure 2. Corresponds to Figure 2.

a. Plot shows % IL-9$^+$ of d8 human Th9 cells restimulated with vehicle (n=7), IL-1β (n=3), IL-18 (n=4), IL-33 (n=4), IL-36α (n=7), or IL-36γ (n=7). **b-c.** Timelines show experimental design; graphs shows % IL-9$^+$ (n=6) for human non-restimulated T cells differentiated as in Fig 1a, with STAT5 inhibitor or STAT6 inhibitor from d0-5 (b) or d5-8 (c). **d-f.** Box plot shows concentration (pg/mL, ELISA) of IL-2 (d), IL-4 (e), and IL-9 (f) in supernatants of human *in vitro* differentiated Th1- or Th9 (d5), or Th2 (d14) cells, after 48h restimulation.. **g,h.** d8 human Th9 cells were restimulated with escalating doses of IL-2 (b) (2, 20, or 200 ng/mL) or IL-4 (c) (6, 60, or 500 ng/mL) (n=3). **i,j.** Representative flow plots (i) and box plot (j) show % IL-9$^+$ cells in resting (d4) murine Th9 cells restimulated with IL-2 + IL-4 (n=10) **k.** Box plot shows pooled results d8 human Th9 cells restimulated with vehicle (n=9), IL-6 (n=3), IL-7 (n=5), IL-12 (n=3), IL-21 (n=3), or TSLP (n=4). **l, m.** Box plots show pooled (n=6) mean fluorescence intensity (MFI) of pSTAT5 **(l)** and pSTAT6 **(m)** in d8 human IL-9$^+$ and IL-9$^-$ Th9 cells restimulated with IL-2, IL-4, or IL-2 + IL-4. **n**. Box

plots show pooled (n=3) % IL-9$^+$ d8 human Th9 cells stimulated with IL-2 and IL-4 in the presence of STAT5 or STAT6 inhibitor. For all experiments: paired or unpaired t-test, normally distributed data; Wilcoxon (paired) or Mann-Whitney (unpaired), non-normally distributed data. Box plots show all data points (min to max, lines at median). All statistical tests are 2-sided, all replicates are biologically independent samples.

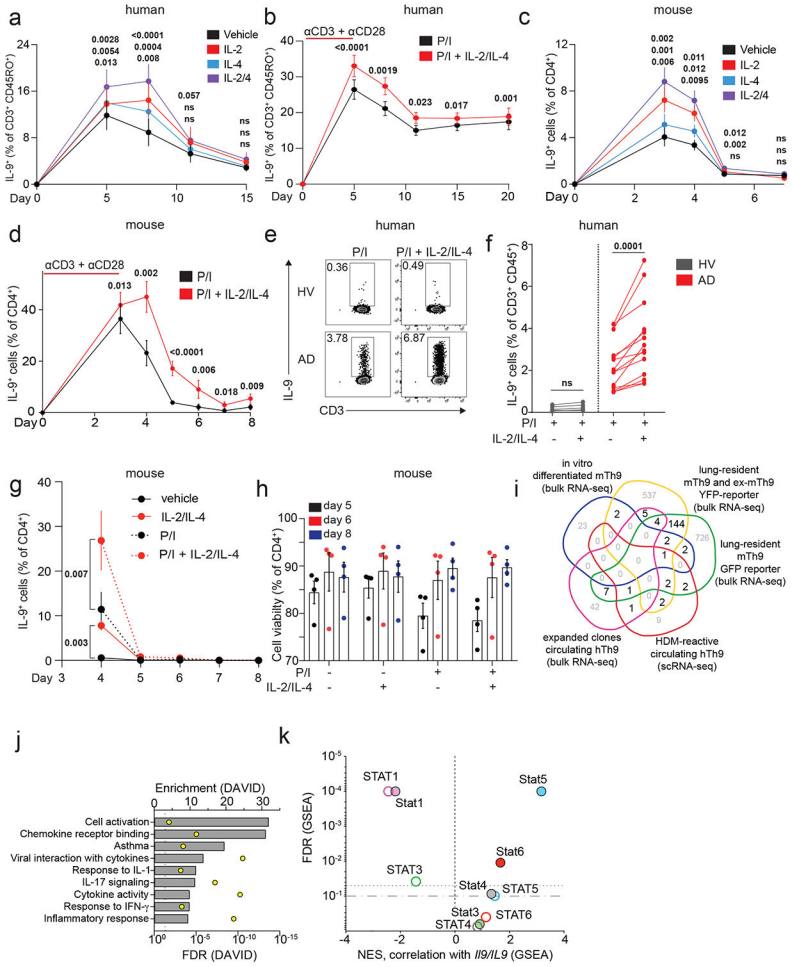

Extended Data Figure 3. Corresponds to Figure 3.

a b. Line graph shows % IL-9$^+$ cells of human Th9 differentiated as in Fig 1a. Cells were restimulated with vehicle, IL-2, IL-4, or IL-2 + IL-4 (**a,** n=6); **b.** on d5 (n=14), d8/d11 (n=17), d15 (n=16), and d20 (n=11), cells were restimulated with PMA + ionomycin (P/I) or P/I + IL-2 + IL-4. **c,d.** Line graph shows % IL-9$^+$ cells of murine Th9 differentiated as in Fig 1d. Cells were restimulated with vehicle, IL-2, IL-4, or IL-2 + IL-4 (**c,** n=4). **d.** On d3 (n=12), d4 (n=11), d5 (n=9), d6 (n=3), d7 (n=3), and d8 (n=6), cells were restimulated P/I or P/I + IL-2 + IL-4. **e, f.** Representative flow plots **(e)** and graphs **(f)** show % IL-9$^+$ of circulating Th9 cells stimulated with P/I or P/I + IL-2 + IL-4, from healthy volunteer (HV, n=5) or atopic patients (AD, n=14). **g**. Line graphs shows pooled results (n=5) for % IL-9$^+$ cells from IL-9 reporter (INFER) mice, sorted on d3 and maintained as in Fig 1d. Cells were restimulated with vehicle, IL-2 + IL-4, P/I or P/I + IL-2 + IL-4, p-value is for d4. **h.** Bar graphs show viability (n=4) for Th9 cells. **i**. Venn diagram

shows generation of “allergic Th9” cassette using: HDM-reactive circulating Th9 cells from allergic patients[1], Th9 clones from healthy subjects[2], pulmonary Th9 cells from IL-9 reporter mice, and *in vitro* differentiated Th9 cells[3]. Genes differentially expressed in >1 dataset were selected. **j.** Bar graph shows pathway enrichment scores and false discovery rates (FDR, DAVID) for the “allergic Th9” cassette. **k**. Scatterplot shows enrichment score (GSEA) and FDR for correlation (Pearson) of STAT1, STAT3, STAT4, STAT5, and STAT6 target genes with murine *Il9* expression and human *IL9* expression. For all experiments: paired or unpaired t-test, normally distributed data; Wilcoxon (paired) or Mann-Whitney (unpaired), non-normally distributed data. Bar/line graphs show mean ± SEM; box plots show all data points (min to max, lines at median). All statistical tests are 2-sided, all replicates are biologically independent samples.

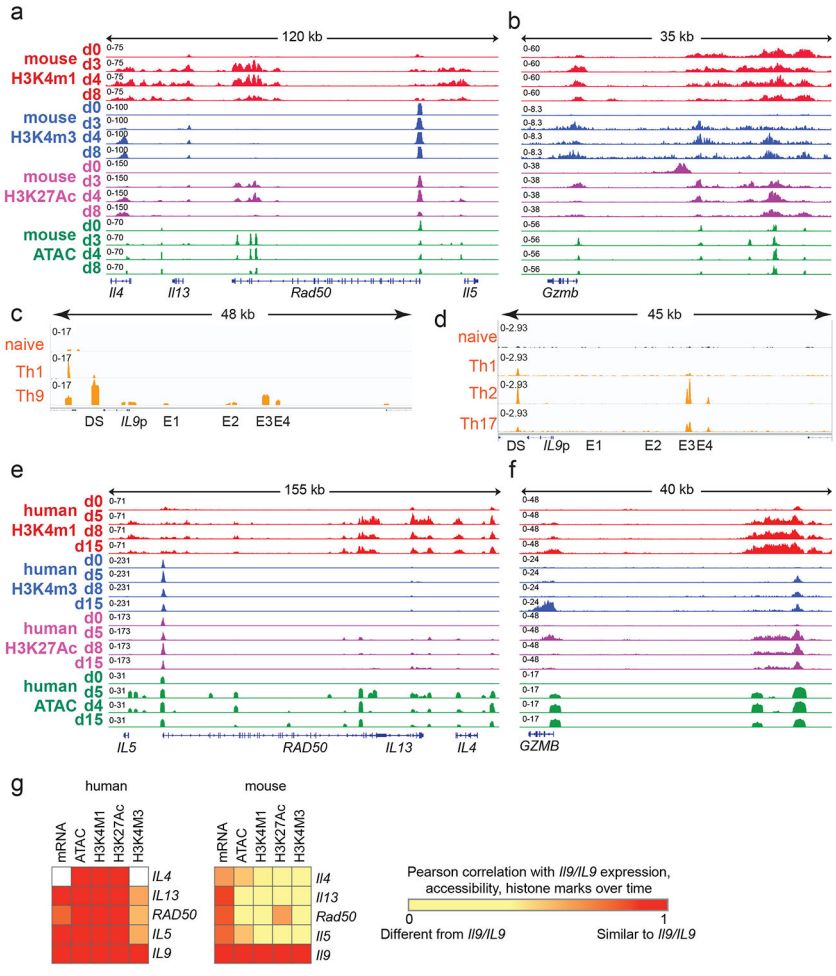

Extended Data Figure 4. Corresponds to Figure 4.

a, b. Genome tracks show poised enhancer (H3K4m1), active promoter (H3K4m3), active enhancer (H3K27Ac) marks, and accessibility (ATAC) of the murine Th2 (**a**, *Il4-Il13-Rad50-Il5*) and *Gzmb* loci at different time points during Th9 differentiation and resting. **c, d**. ATAC-seq tracks show the human extended *IL9* locus including the promoter (Il9p), downstream enhancer (DS) and upstream enhancers 1-4 (E1-E4), in naïve T cells, Th1 cells (d5), and Th9 cells (d5) **(c)**, and in *ex vivo* naïve, Th1, Th2, and Th17 cells from

ENCODE **(d)**. **e, f.** Genome tracks show poised enhancer (H3K4m1), active promoter (H3K4m3), active enhancer (H3K27Ac) marks, and accessibility (ATAC) of the human Th2 (**e**, *IL4-IL13-RAD50-IL5*) and *GZMB* loci at different time points during Th9 differentiation and resting. **g.** Heatmap shows Pearson correlation of *Il9/IL9* expression, ATAC-seq tag density, H3K4me1 tag density, H3K4me3 tag density, and H3K27Ac tag density with those of *Il4/IL4*, *Il13/IL13*, *Rad50/RAD50*, and *Il5/IL5*.

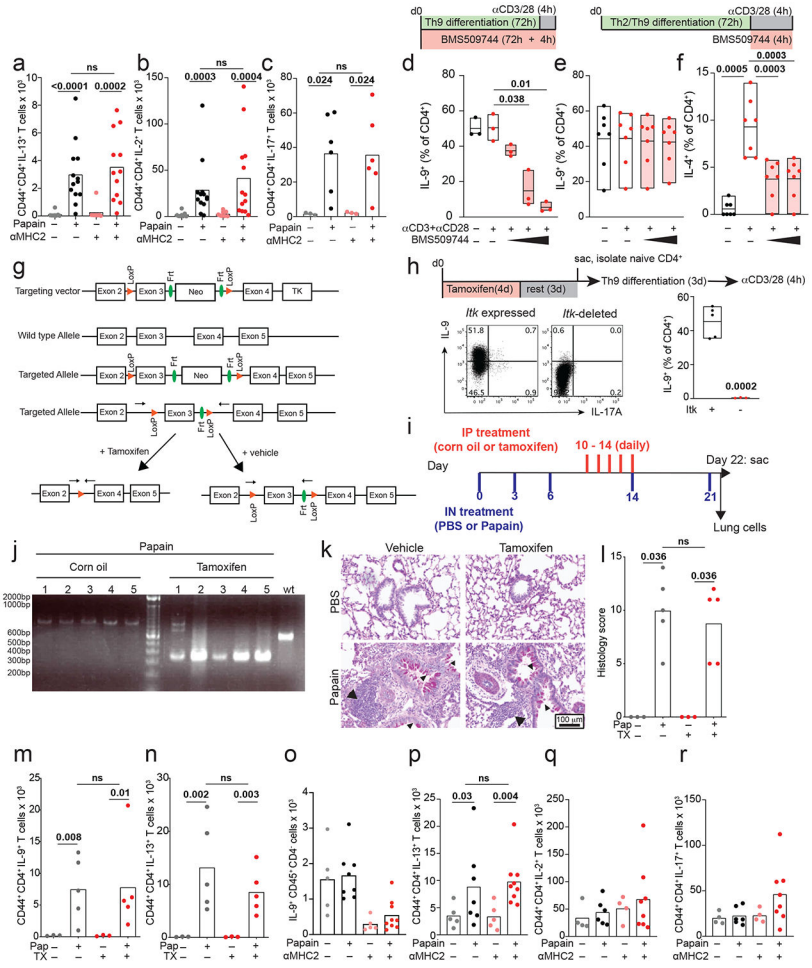

Extended Data Figure 5. Corresponds to Figure 5.

a-c. Pooled counts of pulmonary $CD45^+TCR\beta^+CD4^+CD44^+IL\text{-}13^+$ cells **(a,** n=8, PBS; n=13, papain), $CD45^+TCR\beta^+CD4^+CD44^+IL\text{-}17A^+$ cells (**b,** n=3, PBS; n=6, papain), and $CD45^+TCR\beta^+CD4^+CD44^+IL\text{-}2^+$ cells **(c,** n=8, PBS; n=13, papain) from mice treated with isotype vs. αMHC2 between papain sensitization and challenge. **d.** Th9 cells were differentiated in the presence of vehicle vs. BMS509744 (Itk inhibitor; 0.5 μM, 1 μM, 1.5 μM) and restimulated with αCD3 + αCD28 (n=3) **e-f.** Bar graphs (n=7) show $\%IL\text{-}9^+$ **(e)** of Th9 and $\%IL\text{-}4^+$ **(f)** of Th2 cells restimulated with αCD3 + αCD28 and vehicle vs. BMS509744 (0.5 μM, 1 μM), **g.** Design of inducible Itk-deleted mouse. $Itk^{flox/flox}$ were crossed ERT-Cre mice to generate Itk^{ERT} mice. **h.** Representative flow plot and bar graph show $\%IL\text{-}9^+$ cells of Th9 cells from TAM-treated (Itk-deleted, n = 3) vs. TAM-

untreated (n=5) mice. **i.** Timeline shows model of papain-induced airway inflammation with Itk deletion. Mice were treated with vehicle vs. tamoxifen between sensitization and challenge. **j.** Gel shows that injection of tamoxifen results in deletion of WT *Itk* gene in mice from **(i)**. **k-n.** Representative periodic acid-Schiff (PAS) stained images **(k),** pooled histology scores **(l**, n=3, PBS; n=5, Papain), pulmonary $CD45^+TCR\beta^+CD4^+CD44^+IL\text{-}9^+$ (Th9) **(m**, n=5, PBS; n=10, Papain), and pulmonary $CD45^+TCR\beta^+CD4^+CD44^+IL\text{-}13^+$ (Th2) cell counts **(n**, n=3, PBS; n=5, Papain), from $Itk^{f/f}$ treated with vehicle vs. tamoxifen as in **(i)**. **o-r.** Pooled counts of pulmonary $CD45^+CD4^-$ $IL\text{-}9^+$ cells (**o**, n=5, PBS; n=8, Papain), $CD45^+TCR\beta^+CD4^+CD44^+IL\text{-}13^+$ cells (Th2) **(p**, n=5, PBS; n=8, Papain), $CD45^+TCR\beta^+CD4^+CD44^+IL\text{-}17A^+$ cells (Th17) (**q**, n=4, PBS; n=7, Papain), and $CD45^+TCR\beta^+CD4^+CD44^+IL\text{-}2^+$ cells **(r** n=4, PBS; n=7, Papain) ILC2-deficient mice treated with isotype vs. αMHC2 between papain sensitization and challenge. For all experiments: paired or unpaired t-test, normally distributed data; Wilcoxon (paired) or Mann-Whitney (unpaired), non-normally distributed data. Bar graphs show mean ± SEM; box plots show all data points (min to max, lines at median). All statistical tests are 2-sided, all replicates are biologically independent samples from ≥ 2 independent experiments.

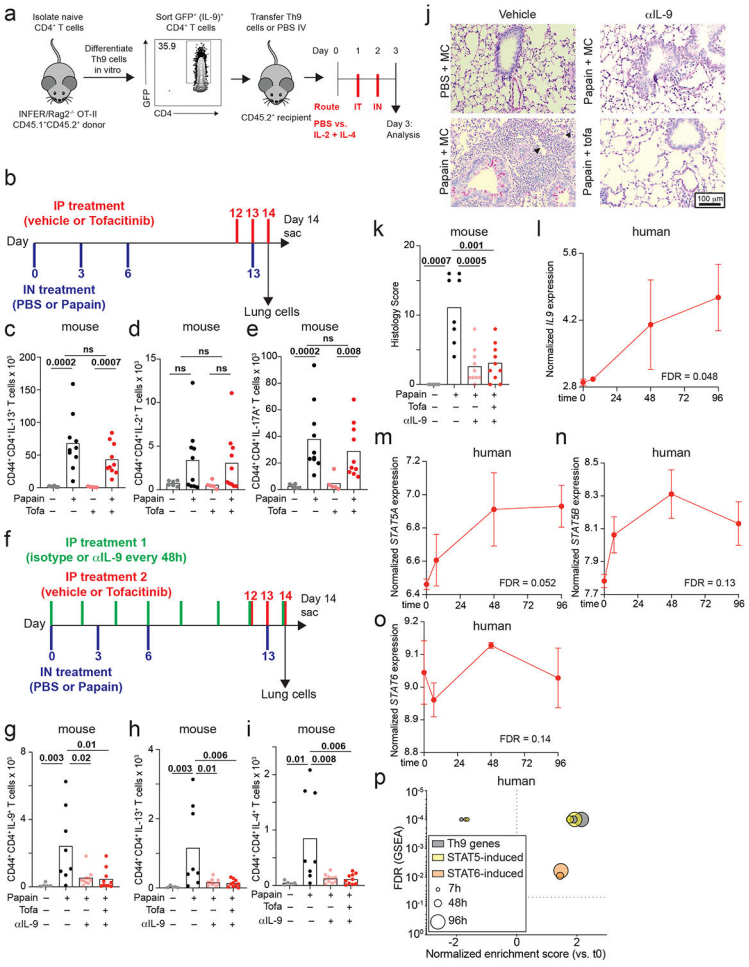

Extended Data Figure 6. Corresponds to Figure 6.

a. Timeline shows Th9 adoptive transfer-induced airway inflammation. Ovalbumin (OVA)-specific OT-ii Th9 cells were differentiated in vitro, sorted for IL-9$^+$ cells, and adoptively transferred. Recipient mice were treated with IL-2 and IL-4 intratracheally and intranasally. **b.** Timeline shows papain-induced airway inflammation with tofacitinib; mice were treated with vehicle vs. tofacitinib between sensitization and challenge. **c-e.** Pooled counts of pulmonary CD45$^+$TCRβ$^+$CD4$^+$CD44$^+$IL-13$^+$ **(c)**, CD45$^+$TCRβ$^+$CD4$^+$CD44$^+$IL-17A$^+$ **(d)**, and CD45$^+$TCRβ$^+$CD4$^+$CD44$^+$IL-2$^+$ cells **(e)** mice treated with vehicle vs. tofacitinib between sensitization and challenge. n=6 (PBS/PBS), 5 (PBS/tofa), 10 (Papain/MC and Papain/tofa) **f.** Timeline shows papain-induced airway inflammation with tofacitinib and αIL-9. Mice were treated as in **(b)** but also received isotype or αIL-9 every other day. **g-k.** Pooled counts of pulmonary CD45$^+$TCRβ$^+$CD4$^+$CD44$^+$IL-9$^+$ **(g)**, CD45$^+$TCRβ$^+$CD4$^+$CD44$^+$IL-13$^+$ **(h)**, and live CD45$^+$TCRβ$^+$CD4$^+$CD44$^+$IL-4$^+$ cells **(i)**, representative periodic acid-Schiff (PAS) stained images **(j)** and pooled histology scores **(k)** of mice treated as in **Fig S6f;** n=5 (PBS/isotype/MC), 8 (Papain/isotype/MC), and 10 (Papain/αIL-9/MC and Papain/αIL-9/tofa). For all *in vivo* experiments: Bar graphs show mean ± SEM; 2-sided Mann-Whitney (unpaired). All replicates are biologically independent samples from ≥ 2 independent experiments. **l-o.** Line graphs show expression (mean ± SEM) over 96 hours of *IL9* **(l)**, *STAT5A* **(m)**, *STAT5B* **(n)**, and *STAT6* **(o)**, in skin of nickel-allergic patients exposed to nickel over 96 hours (n=7) **p**. Graph shows normalized enrichment scores and false discovery rate (GSEA) for expression of “allergic Th9” cassette, STAT5-induced genes, and STAT6-induced genes in 7h-nickel-exposed, 48h-nickel-exposed, and 96h-nickel-exposed skin relative to pre-exposed/unexposed skin.

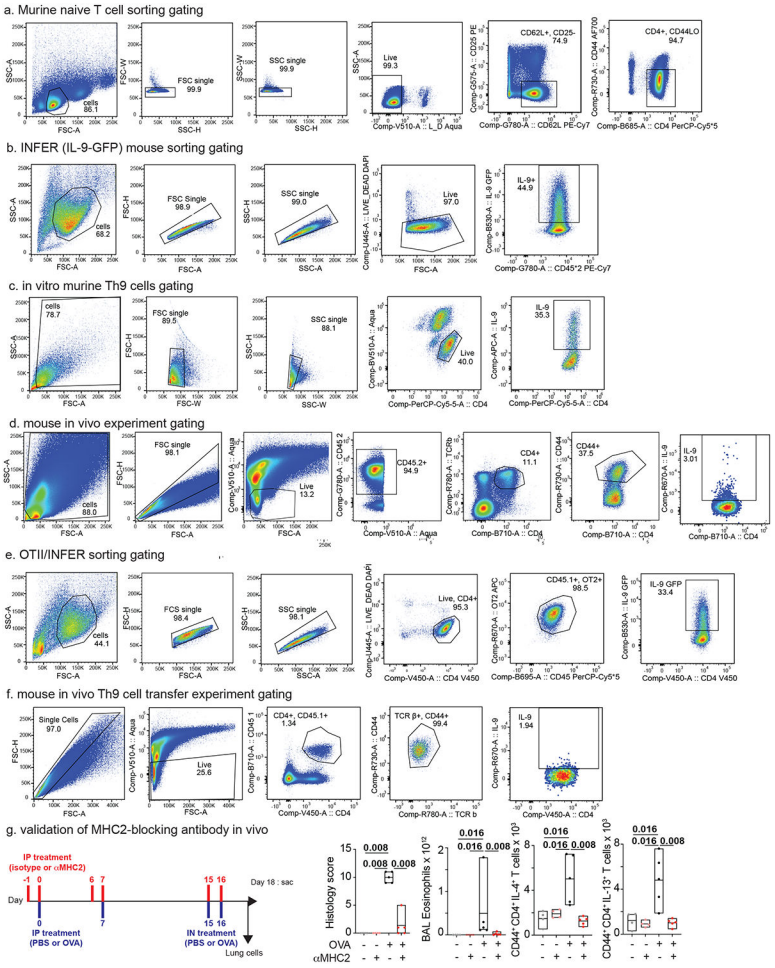

Extended Data Figure 7. Reporting of gating strategy and validation for murine cell studies.

a-f. Representative flow cytometric plots show gating strategies for naïve T cell sorting **(a)**, Th9 sorting for transfer experiments **(b)**, for in vitro differentiated Th9, Th1, and Th2 cells shown in Figures 1-3 and S1-S3 **(c)**, for in vivo memory T helper subsets in Figures 5-6 and S5-S6 **(d-e)**, and for adoptively transferred CD45.1$^+$ Th9 cells analyzed in murine lung two days after transfer **(f)**. **g.** Timeline shows protocol for validation of MHC2 blocking antibody *in vivo*. Mice were sensitized to ovalbumin (OVA) intraperitoneally on d0 and d7, then challenged on d13 and d14. MHC blocking antibody was administered with each dose of OVA. Bar graphs show results of MHC2 validation experiment. Blockade of MHC2 reduced histology scores, BAL Eosinophil counts, and lung-infiltrating IL-4$^+$ and IL-13$^+$ (Th2) cell counts. Mean ± SEM, 2-sided Mann Whitney, all data points represent biological replicates.

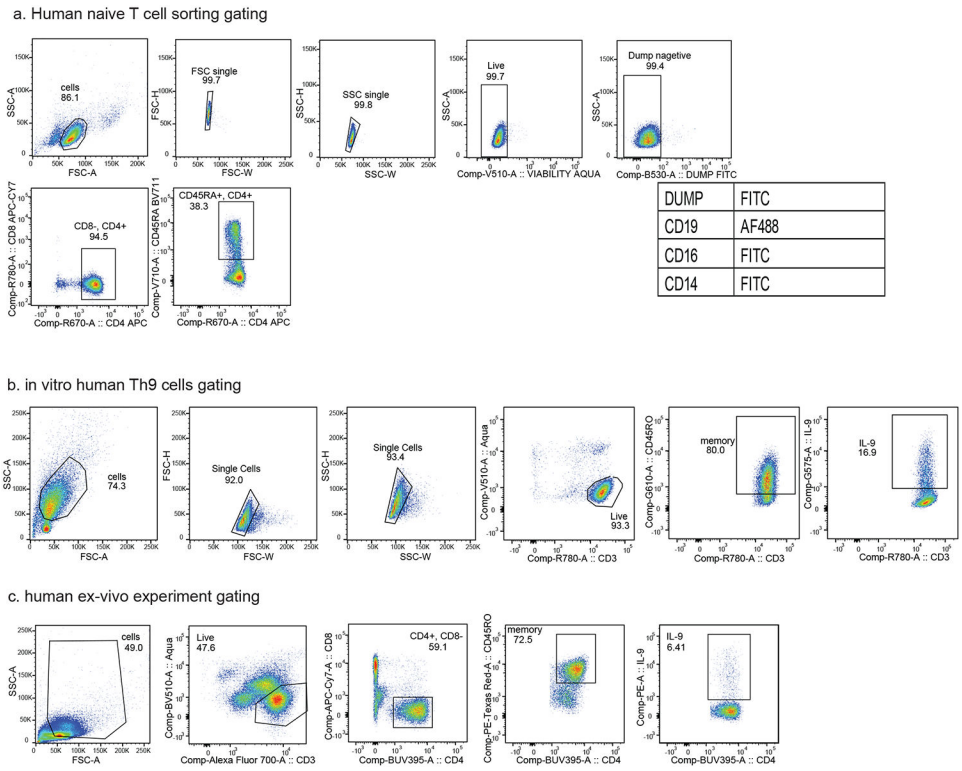

Extended Data Figure 8. Reporting of gating strategy for human cell studies.

Representative flow cytometric plots show gating strategies for naïve T cell sorting (a), gating for in vitro differentiated Th9, Th1, and Th2 cells shown in Figures 1-3 and S1-S3 (b), and for ex vivo circulating memory Th9 cells in stimulated PBMC samples (c).

Extended Data Table 1.

Th9 cassette genes

Murine	Human
Adam15	ADAM15
Anpep	ANPEP
Anxa3	ANXA3
Anxa4	ANXA4
App	APP
Arg1	ARG1
Arg2	ARG2
Atf3	ATF3
Atp6v0c	ATP6V0C
Basp1	BASP1
Batf3	BATF3
Bcl2a1d	BCL2A1
AA467197	C15ORF48

Murine	Human
C4b	C4A
Cav1	CAV1
Cavin1	CAVIN1
Ccl11	CCL11
Ccl12	CCL17
Ccl17	CCL2
Ccl22	CCL22
Ccl24	CCL24
Ccl3	CCL3
Ccl7	CCL7
Ccr1	CCR1
Ccr4	CCR4
Ccr8	CCR8
Cd24a	CD24
Cd300c2	CD300C
Cd63	CD63
Cdc42ep4	CDC42EP4
Cfh	CFH
Cish	CISH
Clec4a3	CLEC4C
Clec4d	CLEC4D
Clic4	CLIC4
Clu	CLU
Col6a1	COL6A1
Cox17	COX17
Crabp2	CRABP2
Creg1	CREG1
Creld2	CRELD2
Csf2	CSF2
Csf2ra	CSF2RA
Cst3	CST3
Cstb	CSTB
Ctsh	CTSH
Ctsz	CTSZ
Cx3cr1	CX3CR1
Cxcl16	CXCL16
Cxcl2	CXCL3
Cxcl3	CXCL3
Cxcl5	CXCL6

Murine	Human
Cyp11a1	CYP11A1
Cyp4f18	CYP4F2
Dohh	DOHH
Dstn	DSTN
Ece1	ECE1
Egfl7	EGFL7
Eif4ebp1	EIF4EBP1
Emp2	EMP2
Fabp5	FABP5
Fam110a	FAM110A
Fkbp11	FKBP11
Fkbp2	FKBP2
Ftl1	FTL
G0s2	G0S2
Gabarapl1	GABARAPL1
Galk1	GALK1
Gcm1	GCM1
Gcsh	GCSH
Gpx3	GPX3
Gsn	GSN
Gstm1	GSTM5
Gzmb	GZMB
Havcr2	HAVCR2
Hdc	HDC
Hk2	HK2
Hlf	HLF
Hmgn3	HMGN3
Hpgd	HPGD
Hspb1	HSPB1
Hspe1	HSPE1
Idi2	IDI2
Ier3	IER3
Ifi30	IFI30
Ifitm3	IFITM3
Igfbp7	IGFBP7
Il10	IL10
Il13	IL13
Il1r2	IL1R2
Il1rl1	IL1RL1

Murine	Human
Il4	IL4
Il5	IL5
Il9	IL9
Kctd14	KCTD14
Lat2	LAT2
Lcn2	LCN2
Lgmn	LGMN
Litaf	LITAF
Manf	MANF
Map3k8	MAP3K8
Marcks	MARCKS
Mcfd2	MCFD2
Mgll	MGLL
Mgp	MGP
Mgst1	MGST1
Mif	MIF
Mrpl12	MRPL12
Mrpl36	MRPL36
Mrto4	MRTO4
Mt1	MT1G
Mt2	MT2A
Myo1e	MYO1E
Ncs1	NCS1
Ndufc2	NDUFC2
Nek6	NEK6
Nhp2	NHP2
Nipa2	NIPA2
Nkain1	NKAIN1
Nlrp3	NLRP3
Nme1	NME1
Nrgn	NRGN
Nucb2	NUCB2
Nupr1	NUPR1
Olr1	OLR1
Pdzk1ip1	PDZK1IP1
Perp	PERP
Phlda1	PHLDA1
Pla2g7	PLA2G7
Pld4	PLD4

Murine	Human
Plin2	PLIN2
Plk2	PLK2
Pparg	PPARG
Ppic	PPIC
Pth	PTH
Pxdc1	PXDC1
Rai14	RAI14
Retnla	RETNLB
Rgl1	RGL1
Rpph1	RPPH1
Rps27l	RPS27L
S100a1	S100A1
S100a8	S100A8
Sap30	SAP30
Sdc1	SDC1
Sec61b	SEC61B
Sec61g	SEC61G
Sema7a	SEMA7A
Serpina1a	SERPINA1
Slc15a3	SLC15A3
Slc9a3r2	SLC9A3R2
Spi1	SPI1
Sv2c	SV2C
Tfec	TFEC
Thbd	THBD
Thbs1	THBS1
Timm13	TIMM13
Timp1	TIMP1
Tmem220	TMEM220
Tnfsf10	TNFSF10
Tnip3	TNIP3
Trmt1	TRMT1
Trmt61a	TRMT61A
Tubb2a	TUBB2A
Tubb6	TUBB6
Txndc17	TXNDC17
Uqcc2	UQCC2
Uqcr10	UQCR10
Uqcr11	UQCR11

Murine	Human
Vat1	VAT1
Vcam1	VCAM1
Ybx3	YBX3
Yif1a	YIF1A
Zbtb32	ZBTB32
Zeb2	ZEB2

Extended Data Table 2.

Public datasets analyzed

Dataset	Utilization
GSE97087	antitumor Th9,Th1, and Th17
GSE133385	**1** lesional *IL9*^{high} vs. nonlesional *IL9*^{low} atopic dermatitis skin **2** Pre-treatment vs. post-treatment lesional *IL9*^{high} skin (JAK-SYK inhibitor)
GSE73482	**1** House dust mite stimulated T cells from allergic subjects vs. healthy volunteers **2** *IL9*^{high} vs. *IL9*^{low} house dust mite stimulated T cells from allergic subjects
GSE40666	STAT1 target genes
GSE65621	STAT3 target genes
GSE40463	**1** STAT4 target genes **2** STAT6 target genes
GSE77656	STAT5 target genes
GSE39756	IRF4 target genes
GSE64409	NFAT target genes
GSE98413	JunB target genes
GSE6281	Pre-exposure vs. post-exposure skin from nickel-allergic patients exposed to nickel for 96 hours
GSE123501	**1** Th9-specific genes (in vitro differentiated Th9 vs. Th1, Th2, Th17, iTreg) **2** YFP^{+} lung-resident Th9 cells (papain-induced airway inflammation, IL-9 YFP fate reporter) **3** GFP^{+} lung-resident Th9 cells (papain-induced airway inflammation, IL-9 GFP reporter)
E-MTAB-5739	IL-9^{+} T cell clones expanded from PBMC of healthy volunteers
GSE146170	IL-9^{+} house dust mite reactive T helper cells isolated from asthmatic patients

Acknowledgements

The authors would like to thank Richard Flavell and Paula Licona-Limon for generously providing INFER and *Klrg1*^{Cre} mice. We would like to thank Franziska Petermann, Yvonne Baumer, and Shmuel Muallem for their thoughtful review of and comments on the manuscript. We would like to acknowledge the NIAID flow core for their assistance with flow sorting and analysis and the NIAMS sequencing core for assistance with sequencing and analysis. We would like to thank Julie Reilley and Jennifer Cannons for assistance with sample retrieval. The study was funded by the Intramural Research Programs of NIAID and NIAMS. The relevant grants are: ZIA-AI001251 (DMS), ZIA-AI001202 (PAF-G), ZIA-AI001098 (JDM), ZIA-AI001240 (PS), and ZIC-AR041181 (FM).

References

1. Immunology, A. A. o. A. A. a. Allergy Statistics, <https://www.aaaai.org/About/News/For-Media/Allergy-Statistics> (2021).
2. Angkasekwinai P & Dong C IL-9-producing T cells: potential players in allergy and cancer. Nat Rev Immunol 21, 37–48, doi:10.1038/s41577-020-0396-0 (2021). [PubMed: 32788707]
3. Shimbara A et al. IL-9 and its receptor in allergic and nonallergic lung disease: increased expression in asthma. J Allergy Clin Immunol 105, 108–115, doi:10.1016/s0091-6749(00)90185-4 (2000). [PubMed: 10629460]
4. Brough HA et al. IL-9 is a key component of memory TH cell peanut-specific responses from children with peanut allergy. J Allergy Clin Immunol 134, 1329–1338 e1310, doi:10.1016/j.jaci.2014.06.032 (2014). [PubMed: 25112699]
5. Abdelilah S et al. Functional expression of IL-9 receptor by human neutrophils from asthmatic donors: role in IL-8 release. J Immunol 166, 2768–2774, doi:10.4049/jimmunol.166.4.2768 (2001). [PubMed: 11160343]
6. Liu J et al. IL-9 regulates allergen-specific Th1 responses in allergic contact dermatitis. J Invest Dermatol 134, 1903–1911, doi:10.1038/jid.2014.61 (2014). [PubMed: 24487305]
7. Yao W et al. Interleukin-9 is required for allergic airway inflammation mediated by the cytokine TSLP. Immunity 38, 360–372, doi:10.1016/j.immuni.2013.01.007 (2013). [PubMed: 23376058]
8. Wilhelm C et al. An IL-9 fate reporter demonstrates the induction of an innate IL-9 response in lung inflammation. Nat Immunol 12, 1071–1077, doi:10.1038/ni.2133 (2011). [PubMed: 21983833]
9. Licona-Limon P et al. Th9 Cells Drive Host Immunity against Gastrointestinal Worm Infection. Immunity 39, 744–757, doi:10.1016/j.immuni.2013.07.020 (2013). [PubMed: 24138883]
10. Kaplan MH, Hufford MM & Olson MR The development and in vivo function of T helper 9 cells. Nat Rev Immunol 15, 295–307, doi:10.1038/nri3824 (2015). [PubMed: 25848755]
11. Gerlach K et al. TH9 cells that express the transcription factor PU.1 drive T cell-mediated colitis via IL-9 receptor signaling in intestinal epithelial cells. Nat Immunol 15, 676–686, doi:10.1038/ni.2920 (2014). [PubMed: 24908389]
12. Xue G, Jin G, Fang J & Lu Y IL-4 together with IL-1beta induces antitumor Th9 cell differentiation in the absence of TGF-beta signaling. Nat Commun 10, 1376, doi:10.1038/s41467-019-09401-9 (2019). [PubMed: 30914642]
13. Nakatsukasa H et al. The DNA-binding inhibitor Id3 regulates IL-9 production in CD4(+) T cells. Nat Immunol 16, 1077–1084, doi:10.1038/ni.3252 (2015). [PubMed: 26322481]
14. Schlapbach C et al. Human TH9 cells are skin-tropic and have autocrine and paracrine proinflammatory capacity. Sci Transl Med 6, 219ra218, doi:10.1126/scitranslmed.3007828 (2014).
15. Seumois G et al. Single-cell transcriptomic analysis of allergen-specific T cells in allergy and asthma. Sci Immunol 5, doi:10.1126/sciimmunol.aba6087 (2020).
16. Schwartz DM et al. Retinoic Acid Receptor Alpha Represses a Th9 Transcriptional and Epigenomic Program to Reduce Allergic Pathology. Immunity 50, 106–120 e110, doi:10.1016/j.immuni.2018.12.014 (2019). [PubMed: 30650370]
17. Kaplan MH The transcription factor network in Th9 cells. Semin Immunopathol 39, 11–20, doi:10.1007/s00281-016-0600-2 (2017). [PubMed: 27837254]
18. Ulrich BJ et al. Allergic airway recall responses require IL-9 from resident memory CD4(+) T cells. Sci Immunol 7, eabg9296, doi:10.1126/sciimmunol.abg9296 (2022). [PubMed: 35302861]
19. Lee WH et al. BATF3 is sufficient for the induction of Il9 expression and can compensate for BATF during Th9 cell differentiation. Exp Mol Med 51, 1–12, doi:10.1038/s12276-019-0348-6 (2019).
20. Gomez-Rodriguez J et al. Itk is required for Th9 differentiation via TCR-mediated induction of IL-2 and IRF4. Nat Commun 7, 10857, doi:10.1038/ncomms10857 (2016). [PubMed: 26936133]
21. Richard AC et al. The TNF-family ligand TL1A and its receptor DR3 promote T cell-mediated allergic immunopathology by enhancing differentiation and pathogenicity of IL-9-producing T cells. J Immunol 194, 3567–3582, doi:10.4049/jimmunol.1401220 (2015). [PubMed: 25786692]

22. Xiao X et al. OX40 signaling favors the induction of T(H)9 cells and airway inflammation. Nat Immunol 13, 981–990, doi:10.1038/ni.2390 (2012). [PubMed: 22842344]
23. Micosse C et al. Human "TH9" cells are a subpopulation of PPAR-gamma(+) TH2 cells. Sci Immunol 4, doi:10.1126/sciimmunol.aat5943 (2019).
24. Liao W et al. Opposing actions of IL-2 and IL-21 on Th9 differentiation correlate with their differential regulation of BCL6 expression. Proc Natl Acad Sci U S A 111, 3508–3513, doi:10.1073/pnas.1301138111 (2014). [PubMed: 24550509]
25. Fu Y et al. STAT5 promotes accessibility and is required for BATF-mediated plasticity at the Il9 locus. Nat Commun 11, 4882, doi:10.1038/s41467-020-18648-6 (2020). [PubMed: 32985505]
26. Harusato A et al. IL-36gamma signaling controls the induced regulatory T cell-Th9 cell balance via NFkappaB activation and STAT transcription factors. Mucosal Immunol 10, 1455–1467, doi:10.1038/mi.2017.21 (2017). [PubMed: 28327619]
27. Dardalhon V et al. IL-4 inhibits TGF-beta-induced Foxp3+ T cells and, together with TGF-beta, generates IL-9+ IL-10+ Foxp3(−) effector T cells. Nat Immunol 9, 1347–1355, doi:10.1038/ni.1677 (2008). [PubMed: 18997793]
28. Olson MR et al. Paracrine IL-2 Is Required for Optimal Type 2 Effector Cytokine Production. J Immunol 198, 4352–4359, doi:10.4049/jimmunol.1601792 (2017). [PubMed: 28468971]
29. Harnett W & Harnett MM Helminth-derived immunomodulators: can understanding the worm produce the pill? Nat Rev Immunol 10, 278–284, doi:10.1038/nri2730 (2010). [PubMed: 20224568]
30. Guo L et al. IL-1 family members and STAT activators induce cytokine production by Th2, Th17, and Th1 cells. Proc Natl Acad Sci U S A 106, 13463–13468, doi:10.1073/pnas.0906988106 (2009). [PubMed: 19666510]
31. Canaria DA et al. IL-1beta promotes IL-9-producing Th cell differentiation in IL-2-limiting conditions through the inhibition of BCL6. Front Immunol 13, 1032618, doi:10.3389/fimmu.2022.1032618 (2022). [PubMed: 36389679]
32. Luo Y et al. JAK-STAT signaling in human disease: From genetic syndromes to clinical inhibition. J Allergy Clin Immunol 148, 911–925, doi:10.1016/j.jaci.2021.08.004 (2021). [PubMed: 34625141]
33. Wang Y et al. Germinal-center development of memory B cells driven by IL-9 from follicular helper T cells. Nat Immunol 18, 921–930, doi:10.1038/ni.3788 (2017). [PubMed: 28650481]
34. Salerno F et al. Translational repression of pre-formed cytokine-encoding mRNA prevents chronic activation of memory T cells. Nat Immunol 19, 828–837, doi:10.1038/s41590-018-0155-6 (2018). [PubMed: 29988089]
35. Zhang Y et al. Human TH9 differentiation is dependent on signal transducer and activator of transcription (STAT) 3 to restrain STAT1-mediated inhibition. J Allergy Clin Immunol 143, 1108–1118 e1104, doi:10.1016/j.jaci.2018.06.036 (2019). [PubMed: 30030006]
36. Canaria DA et al. STAT5 Represses a STAT3-Independent Th17-like Program during Th9 Cell Differentiation. J Immunol 207, 1265–1274, doi:10.4049/jimmunol.2100165 (2021). [PubMed: 34348976]
37. Olson MR, Verdan FF, Hufford MM, Dent AL & Kaplan MH STAT3 Impairs STAT5 Activation in the Development of IL-9-Secreting T Cells. J Immunol 196, 3297–3304, doi:10.4049/jimmunol.1501801 (2016). [PubMed: 26976954]
38. Shih HY et al. Developmental Acquisition of Regulomes Underlies Innate Lymphoid Cell Functionality. Cell 165, 1120–1133, doi:10.1016/j.cell.2016.04.029 (2016). [PubMed: 27156451]
39. Heinz S et al. Simple combinations of lineage-determining transcription factors prime cis-regulatory elements required for macrophage and B cell identities. Mol Cell 38, 576–589, doi:10.1016/j.molcel.2010.05.004 (2010). [PubMed: 20513432]
40. Abdul Qayum A et al. The Il9 CNS-25 Regulatory Element Controls Mast Cell and Basophil IL-9 Production. J Immunol 203, 1111–1121, doi:10.4049/jimmunol.1900272 (2019). [PubMed: 31350354]
41. Xiao X et al. Guidance of super-enhancers in regulation of IL-9 induction and airway inflammation. J Exp Med 215, 559–574, doi:10.1084/jem.20170928 (2018). [PubMed: 29339447]

42. Koh B et al. A conserved enhancer regulates Il9 expression in multiple lineages. Nat Commun 9, 4803, doi:10.1038/s41467-018-07202-0 (2018). [PubMed: 30442929]
43. Guo L et al. Innate immunological function of TH2 cells in vivo. Nat Immunol 16, 1051–1059, doi:10.1038/ni.3244 (2015). [PubMed: 26322482]
44. Pavel AB et al. Oral Janus kinase/SYK inhibition (ASN002) suppresses inflammation and improves epidermal barrier markers in patients with atopic dermatitis. J Allergy Clin Immunol 144, 1011–1024, doi:10.1016/j.jaci.2019.07.013 (2019). [PubMed: 31356921]
45. Lu Y et al. Th9 Cells Represent a Unique Subset of CD4(+) T Cells Endowed with the Ability to Eradicate Advanced Tumors. Cancer Cell 33, 1048–1060 e1047, doi:10.1016/j.ccell.2018.05.004 (2018). [PubMed: 29894691]
46. Chopp L, Redmond C, O'Shea JJ & Schwartz DM From thymus to tissues and tumors: A review of T-cell biology. J Allergy Clin Immunol, doi:10.1016/j.jaci.2022.10.011 (2022).
47. Joyce JA & Fearon DT T cell exclusion, immune privilege, and the tumor microenvironment. Science 348, 74–80, doi:10.1126/science.aaa6204 (2015). [PubMed: 25838376]
48. Elyaman W & Khoury SJ Th9 cells in the pathogenesis of EAE and multiple sclerosis. Semin Immunopathol 39, 79–87, doi:10.1007/s00281-016-0604-y (2017). [PubMed: 27844107]
49. Caucheteux SM et al. IL-1beta enhances inflammatory TH2 differentiation. J Allergy Clin Immunol 138, 898–901 e894, doi:10.1016/j.jaci.2016.02.033 (2016). [PubMed: 27212084]
50. Ansel KM, Djuretic I, Tanasa B & Rao A Regulation of Th2 differentiation and Il4 locus accessibility. Annu Rev Immunol 24, 607–656, doi:10.1146/annurev.immunol.23.021704.115821 (2006). [PubMed: 16551261]

Methods-only References

51. Herndler-Brandstetter D et al. KLRG1(+) Effector CD8(+) T Cells Lose KLRG1, Differentiate into All Memory T Cell Lineages, and Convey Enhanced Protective Immunity. Immunity 48, 716–729 e718, doi:10.1016/j.immuni.2018.03.015 (2018). [PubMed: 29625895]
52. Zhu J et al. Conditional deletion of Gata3 shows its essential function in T(H)1-T(H)2 responses. Nat Immunol 5, 1157–1165, doi:10.1038/ni1128 (2004). [PubMed: 15475959]
53. Gurram RK et al. Crosstalk between ILC2s and Th2 cells varies among mouse models. Cell Rep 42, 112073, doi:10.1016/j.celrep.2023.112073 (2023). [PubMed: 36735533]
54. Liu P, Jenkins NA & Copeland NG A highly efficient recombineering-based method for generating conditional knockout mutations. Genome Res 13, 476–484, doi:10.1101/gr.749203 (2003). [PubMed: 12618378]
55. Corces MR et al. An improved ATAC-seq protocol reduces background and enables interrogation of frozen tissues. Nat Methods 14, 959–962, doi:10.1038/nmeth.4396 (2017). [PubMed: 28846090]
56. Buenrostro JD, Wu B, Chang HY & Greenleaf WJ ATAC-seq: A Method for Assaying Chromatin Accessibility Genome-Wide. Curr Protoc Mol Biol 109, 21 29 21–21 29 29, doi:10.1002/0471142727.mb2129s109 (2015).
57. Subramanian A et al. Gene set enrichment analysis: a knowledge-based approach for interpreting genome-wide expression profiles. Proc Natl Acad Sci U S A 102, 15545–15550, doi:10.1073/pnas.0506580102 (2005). [PubMed: 16199517]
58. Mootha VK et al. PGC-1alpha-responsive genes involved in oxidative phosphorylation are coordinately downregulated in human diabetes. Nat Genet 34, 267–273, doi:10.1038/ng1180 (2003). [PubMed: 12808457]
59. Davis CA et al. The Encyclopedia of DNA elements (ENCODE): data portal update. Nucleic Acids Res 46, D794–D801, doi:10.1093/nar/gkx1081 (2018). [PubMed: 29126249]

References

1. Seumois G et al. Single-cell transcriptomic analysis of allergen-specific T cells in allergy and asthma. Sci Immunol 5, doi:10.1126/sciimmunol.aba6087 (2020).

2. Micosse C et al. Human "TH9" cells are a subpopulation of PPAR-gamma(+) TH2 cells. Sci Immunol 4, doi:10.1126/sciimmunol.aat5943 (2019).

3. Schwartz DM et al. Retinoic Acid Receptor Alpha Represses a Th9 Transcriptional and Epigenomic Program to Reduce Allergic Pathology. Immunity 50, 106–120 e110, doi:10.1016/j.immuni.2018.12.014 (2019). [PubMed: 30650370]

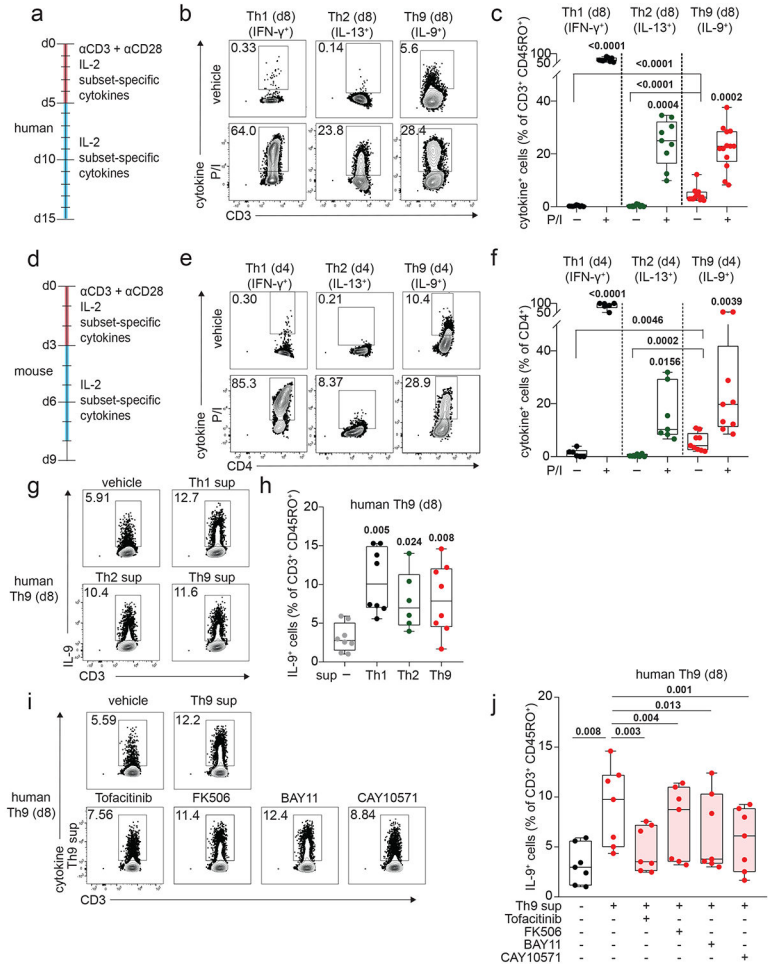

Figure 1. Resting Th9 cells uniquely produce IL-9 independent of T cell receptor (TCR) restimulation, downstream of paracrine STAT-dependent cytokines.

a. Timeline shows differentiation protocol for human T helper cells. Naïve CD4$^+$ T cells from healthy volunteers were activated for 5 days with αCD3, αCD28, IL-2, and subset-promoting cytokines and antibodies. After 5 days, αCD3/αCD28 were withdrawn, and cells were cultured with IL-2 and subset-promoting cytokines and antibodies. **b, c.** Representative flow plot **(b)** and summary data **(c)** for % of cytokine production in human resting (d8, rested for 3 days) Th1 (IFN-γ^+, n = 9), Th2 (IL-13$^+$, n = 9), and Th9 (IL-9$^+$, n = 13) with or without PMA and Ionomycin (P/I). **d.** Timeline shows differentiation protocol for murine T helper cells. Naïve CD4$^+$ T cells from WT C57BL/6 mice were activated for 3 days with αCD3, αCD28, IL-2, and subset-promoting cytokines and antibodies. After 3 days, αCD3/αCD28 were withdrawn, and cells were cultured with IL-2 and subset-promoting cytokines and antibodies. **e, f.** Representative flow plot **(e)** and summary data **(f)** for % of cytokine production in resting (d4) murine Th1 (IFN-γ^+, n = 3), Th2 (IL-13$^+$, n = 4), and Th9 (IL-9$^+$, n = 9) cells restimulated with vehicle control vs. P/I. **g, h.** Representative flow plots **(g)** and summary data **(h)** show % IL-9$^+$ cells of resting (d8) human Th9 cells restimulated with supernatants from Th1 (n = 8), Th2 (n = 6), and Th9 (n = 8) cells. **i, j.** Representative flow cytometry plot **(i)** and summary data **(j)** show % IL-9$^+$ cells of resting (d8) human Th9 cells restimulated with Th9 supernatants in the presence of

vehicle, tofacitinib (JAK-STAT inhibitor), FK506 (calcineurin/NFAT inhibitor), BAY11 (NF-κB inhibitor), or CAY10571 (p38 MAPK inhibitor) (n = 7). For all experiments: paired or unpaired t-test, normally distributed data; Wilcoxon (paired) or Mann-Whitney (unpaired), non-normally distributed data. Box plots show all data points (min to max, lines at median). All statistical tests are 2-sided, all replicates are biologically independent samples.

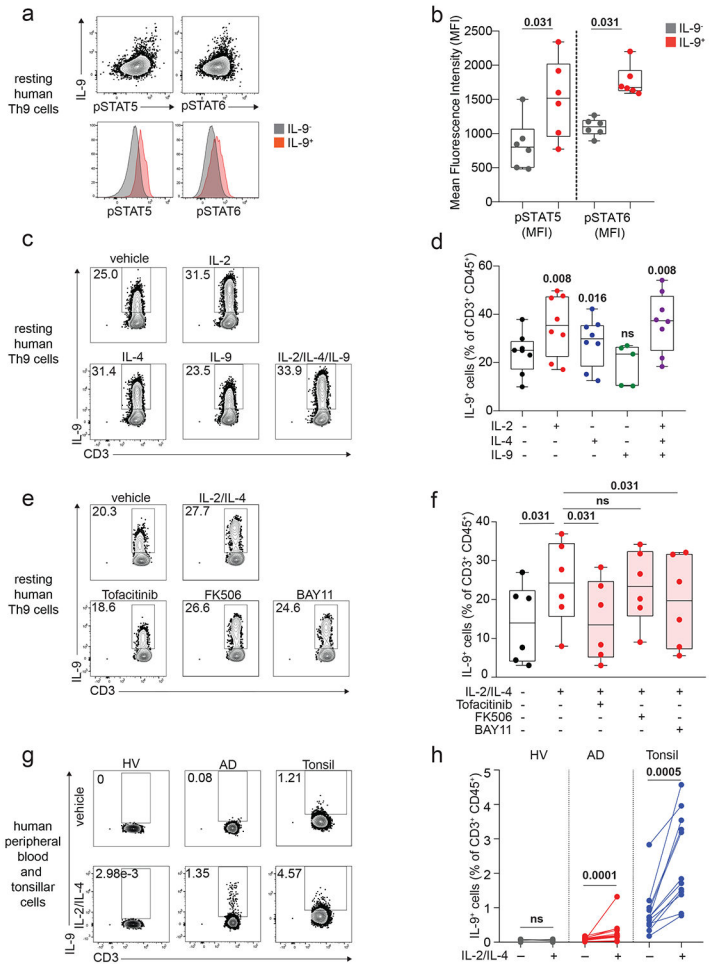

Figure 2. IL-2 and IL-4 rapidly induce bystander activation of resting Th9 cells through STAT5 and STAT6.

a, b. Representative flow plots **(a)** show pSTAT5, pSTAT6, and IL-9 expression in non-restimulated resting (d8 from start of culture) human cells differentiated from naïve T cells under Th9-promoting conditions (IL-2, IL-4, TGF-β, IL-1β, αIFN-γ). Representative histograms **(a)** and summary data **(b)** show mean fluorescence intensity (MFI) of pSTAT5 and pSTAT6 in resting human IL-9$^+$ and IL-9$^-$ cells differentiated under Th9-promoting conditions. Bar graphs show pooled results (n = 6). **c, d.** Representative cytometry plot (**c**) and summary data (**d**) show % IL-9$^+$ cells of resting (d8 from start of culture) human Th9 cells restimulated for 6 hours with vehicle, hIL-2 (n = 8), hIL-4 (n = 8),h IL-9 (n = 5), or a combination of the three (n = 8). **e, f.** Representative flow cytometric plot (**e**) and summary data (**f**) show % IL-9$^+$ cells of resting (d8) human Th9 cells restimulated for 6 hours with IL-2 + IL-4 in the presence of vehicle, tofacitinib (JAK-STAT inhibitor), FK506 (calcineurin/NFAT inhibitor), BAY11 (NF-κB inhibitor), or CAY10571 (p38 MAPK inhibitor) (n = 6). **g, h.** Representative flow cytometric plot (**g**) and summary data (**h**) show % IL-9$^+$ cells of circulating memory CD4$^+$ T cells (CD3$^+$/CD4$^+$/CD8$^-$/CD45RO$^+$ cells) stimulated with vehicle vs. IL-2 + IL-4. Cells derive from healthy volunteer peripheral blood mononuclear cells (HV PBMC, n = 6), atopic dermatitis patient PBMC (AD, n = 14), and HV tonsils (n = 12). For all experiments: paired or unpaired t-test, normally distributed

data; Wilcoxon (paired) or Mann-Whitney (unpaired), non-normally distributed data. Box plots show all data points (min to max, lines at median). All statistical tests are 2-sided, all replicates are biologically independent samples.

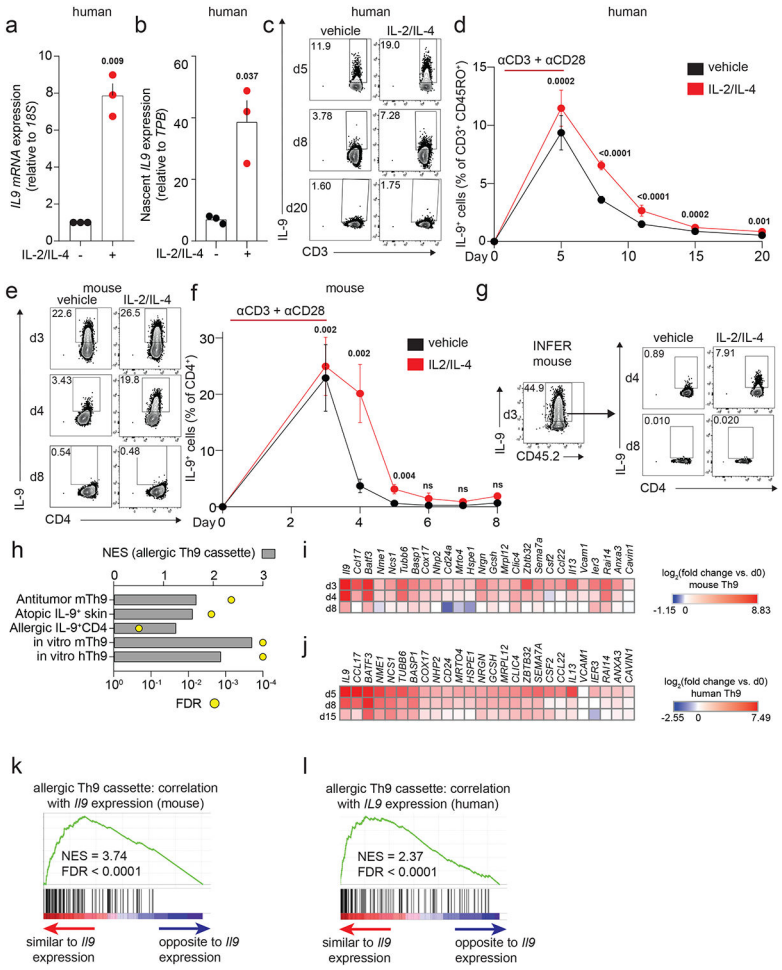

Figure 3. STAT-dependent cytokines induce *IL9* transcription in recently activated Th9 cells.

a, b. Graphs show total **(a)** and nascent **(b)** *IL9* expression in d8 human Th9 cells treated with vehicle or IL-2 + IL-4. (n = 3). **c, d.** Representative flow plots **(c)** and graphs **(d)** show % IL-9$^+$ cells of human Th9 differentiated with αCD3/αCD28 for 5 days then continued with Th9-promoting cytokines/antibodies, but without αCD3/αCD28. On d5 (n = 14), d8/d11 (n = 17), d15 (n = 16), and d20 (n = 11), cells were restimulated with vehicle or IL-2 + IL-4. **e, f.** Representative flow plots **(e)** and graphs **(f)** show % IL-9$^+$ cells of murine Th9 differentiated with αCD3/αCD28 for 3 days, then continued with other Th9-promoting cytokines/antibodies, but without αCD3/αCD28. On d3 (n = 12), d4 (n = 11), d5 (n = 9), d6 (n = 3), d7 (n = 3), and d8 (n = 6), cells were restimulated with vehicle or IL-2 + IL-4. **g.** Representative flow plots show % IL-9$^+$ cells from IL-9 reporter (INFER) mice. IL-9$^+$ cells were sorted on d3 and maintained in Th9-promoting conditions without αCD3/αCD28. Cells were restimulated on d4 and d8 with vehicle or IL-2 + IL-4. **h**. Graph shows normalized enrichment score (NES) and false discovery rate (FDR) of Th9 cassette (GSEA) in antitumor Th9 cells; *IL9*^{high} atopic dermatitis skin; house-dust-mite-stimulated T cells from allergic subjects; d3-murine *in vitro* differentiated Th9; d5-human *in vitro* differentiated Th9. **i,j.** Heatmaps show average fold-change in gene expression of *in vitro* differentiated murine (n = 3, **i**) and human (n = 4, **j**) Th9 cells vs. naïve T cells at various

time points, for “allergic Th9” genes with dynamic enrichment (FC > 2, FDR < 0.05) in murine (d3/4 vs. d0/8) and human (d5/8 vs. d0/15) cells. **k,l**. Enrichment plots show Pearson correlation of “allergic Th9” genes with *Il9/IL9* expression over time in murine (**k**) and human (**l**) Th9 cells. For all experiments: paired or unpaired t-test, normally distributed data; Wilcoxon (paired) or Mann-Whitney (unpaired), non-normally distributed data. For boxplots/line graphs, error bars show ± SEM. All statistical tests are 2-sided, all replicates are biologically independent samples.

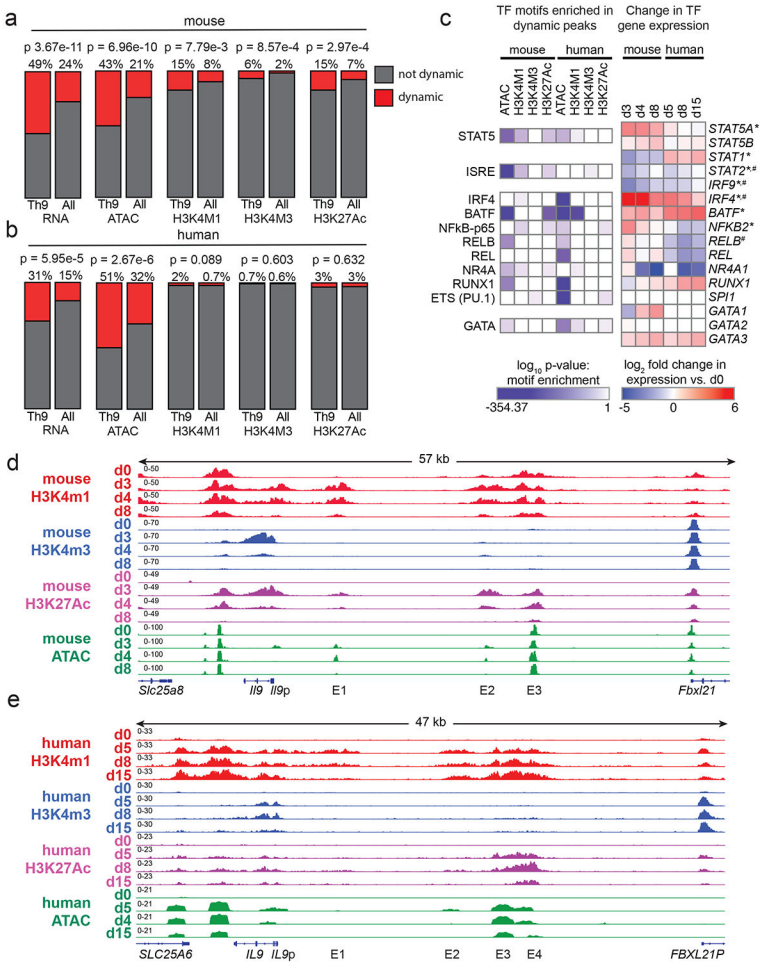

Figure 4. Prolonged resting of Th9 cells reduces accessibility of STAT5 binding sites and type 2 cytokine loci, including critical *IL9* enhancers.

a,b. Bar graphs show enrichment (2-sided Fisher's t-test) in murine (a) and human (b) Th9 cells of dynamically expressed genes, dynamic ATAC-seq (accessibility) peaks, dynamic H3K4Me1 (poised enhancer) peaks, dynamic H3K4Me3 (active promoter) peaks, and dynamic H3K27Ac (active enhancer) peaks in loci/genes mapping to the 'allergic Th9" cassette vs. all coding gene loci. **c.** Heatmap (left) shows log (p-value, HOMER *de novo* motif discovery) for motif enrichment of transcription factors (TF) in human and murine dynamic peaks. All motifs with significant enrichment in at least 1 murine peak set and at least 1 human peak set are shown. Heatmap (right) shows $\log_2$ (average fold-change) in gene expression of TFs with motif enrichment in dynamic peaks. Values are shown for murine and human Th9 at various time points vs. naïve T cells. * transiently upregulated in murine Th9 (FC >2, FDR < 0.05, d3-d4 vs. d0-d8) # transiently upregulated in human Th9 (FC >2, FDR < 0.05, d5-d8 vs. d0-d15); **d, e.** Genome tracks show poised enhancer (H3K4Me1), active promoter (H3K4Me3), active enhancer (H3K27Ac) marks, and accessibility (ATAC) of the murine *Il9* (d) and human *IL9* (e) extended locus including the promoter (*Il9*p), downstream enhancer (DS) and upstream enhancers 1-4 (E1-E4), at different time points during Th9 differentiation and resting. All replicates are biologically independent samples.

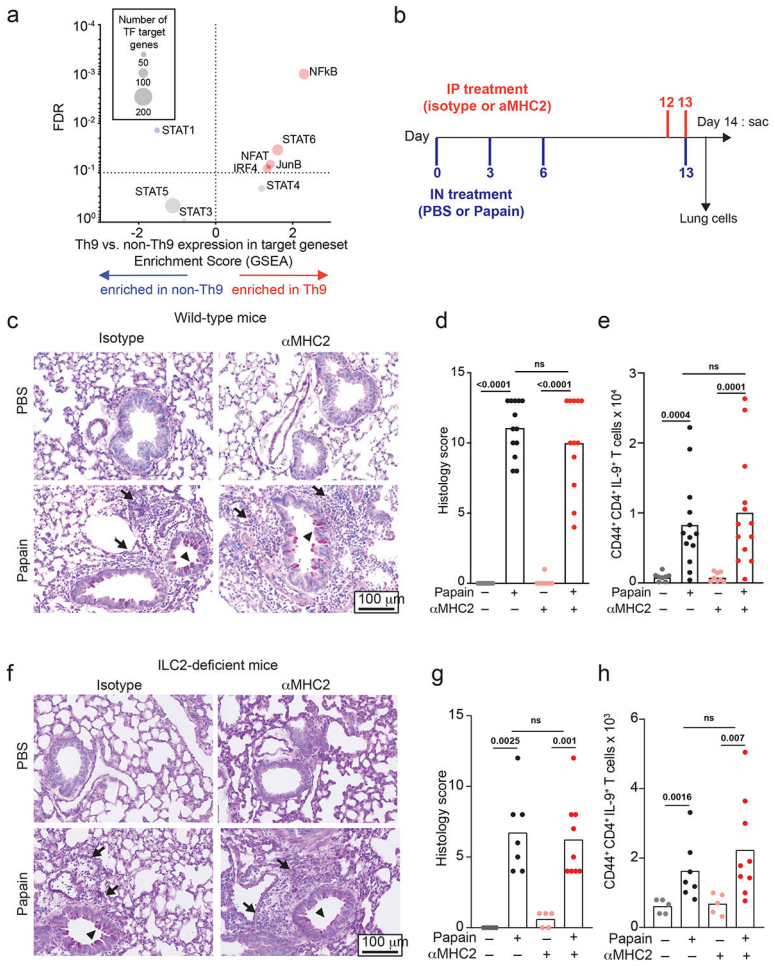

Figure 5. Th9 cells promote TCR-independent airway pathology *in vivo*.

a. Enrichment plots show a normalized enrichment score and FDR (GSEA) for the average, or net, transcriptome of Th9 vs. non-Th9 cells for the following Th9-related and activation-dependent transcription factors (TFs): STAT1, STAT3, STAT4, STAT5, STAT6, IRF4, ,NF-kB[16], NFAT, and JunB. A positive score indicates enrichment in Th9 cells, and a negative score indicates enrichment in non-Th9 cells. A neutral score indicates no significant enrichment. **b**. Timeline shows model of papain-induced airway inflammation with MHC2 blockade. Mice were sensitized and rechallenged with intranasal papain, and treated with isotype vs. αMHC2 during rechallenge. **c-e.** Representative periodic acid-Schiff (PAS) stained images **(c)**, pooled histology scores **(d)**, and live $CD45^+TCR\beta^+CD4^+CD44^+IL\text{-}9^+$ (Th9) cell counts **(h)** from lungs of mice exposed to papain and treated with isotype vs. αMHC II as in **(b)** (arrows, inflammatory infiltrate; triangles, mucus; n= 8, PBS; n = 13, Papain) **f-h.** Representative periodic acid-Schiff (PAS) stained images **(e),** pooled histology scores **(f)**, and live $CD45^+TCR\beta^+CD4^+CD44^+IL\text{-}9^+$ (Th9) cell counts **(h)** from lungs of Type 2 innate lymphoid cell (ILC2) deficient mice exposed to papain and treated with αMHC II or isotype as in **(b)** (arrows, inflammatory infiltrate; triangles, mucus; n= 5, PBS; n = 7, Papain-iso; n = 9, Papain-αMHCII. For all *in vivo* experiments, statistical tests are

2-sided Mann-Whitney; all data are biologically independent samples from ≥ 2 replicate experiments.

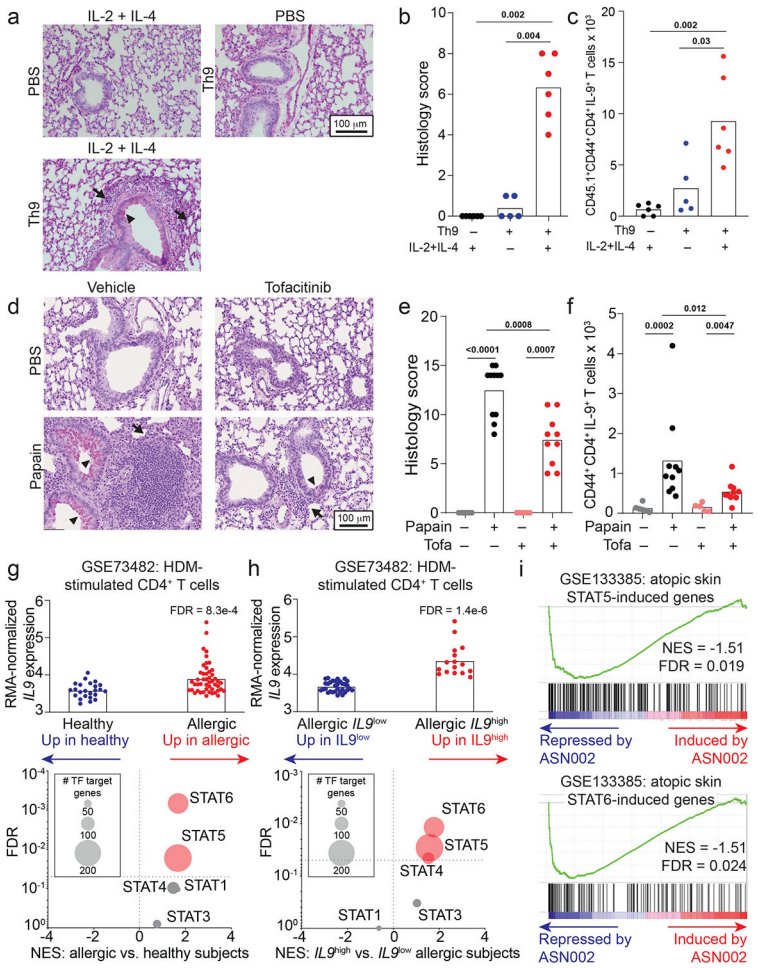

Figure 6. STAT-dependent Th9 bystander activation promotes allergic disease and is associated with responsiveness to JAK inhibitors.

a-c. Representative periodic acid-Schiff (PAS) stained images **(a),** pooled histology scores **(b),** and live CD45.1^{+}TCRβ^{+}CD4^{+}CD44^{+}IL-9^{+} (adoptively transferred Th9) cell counts **(c)** in lungs of WT mice who underwent adoptive transfer of PBS or Th9 cells from congenic donors, followed by intratracheal and intranasal challenge with PBS or IL-2 + IL-4; 3 replicates, n = 2 per replicate; arrows, inflammatory infiltrate; triangles, mucus. **d-f.** Representative PAS-stained images **(d),** pooled histology scores **(e)**, and live CD45^{+}TCRβ^{+}CD4^{+}CD44^{+}IL-9^{+} (Th9) cell counts **(f)** from lungs of mice exposed to chronic papain-induced airway inflammation and treated with methylcellulose (MC) or tofacitinib; n = 6 (PBS/MC), n = 5 (PBS/tofa), n = 11 (Papain/MC), n = 10 (Papain/tofa); arrows, inflammatory infiltrate; triangles, mucus. *In vivo* data are shown as mean ± SEM, Mann-Whitney. **g.** Bar graph shows RMA-normalized *IL9* expression in house dust mite (HDM) treated CD4^{+} T cells from healthy volunteers vs. patients with allergic disease. Scatterplot shows normalized enrichment scores (NES; Gene Set Enrichment Analysis, GSEA) and FDR for genes induced by the following TFs in allergic vs. healthy CD4^{+} cells: STAT1; STAT3; STAT4; STAT5; STAT6. **h.** Bar graph shows RMA-normalized *IL9* expression in HDM-treated CD4^{+} T cells from allergic patients in which *IL9* expression is lower than mean expression for the dataset (*IL9*^{low}) vs. higher than mean for the dataset

(*IL9*^{high}). Scatterplot shows NES (GSEA) and FDR for genes induced by STAT1, STAT3, STAT4, STAT5, and STAT6 in *IL9*^{low} vs. *IL9*^{high} CD4^{+} cells. **i.** GSEA plots show NES and FDR for STAT5- and STAT6-induced genes in d29 vs. d0 skin from AD patients treated with the JAK-SYK inhibitor ASN002, 80 mg daily. All statistical tests are 2-sided; all replicates are biologically independent samples.